J. Indian Inst. Sci., Sept.–Oct. 2000, 80, 437–456.

Rotor side control of grid-connected wound rotor induction machine

RAJIB DATTA* AND V. T. RANGANATHAN**
Department of Electrical Engineering, Indian Institute of Science, Bangalore 560 012, India
*rdatta@ee.iisc.ernet.in; **vtran@ee.iisc.ernet.in

Received on June 26, 2000.

Abstract

This paper deals with modeling, simulation and implementation of rotor side control strategies for a grid-connected wound rotor induction machine. In the system under consideration, the stator is directly connected to the constant frequency three-phase grid and the rotor is supplied by two back-to-back three-phase voltage source inverters with a common DC link. Such a configuration is attractive in large power applications with limited speed range of operation. The rotor currents are controlled at any desired phase, frequency and magnitude to control the active and reactive powers of the machine independently. A stator flux-oriented model of the doubly fed wound rotor induction machine is presented. The current controllers are designed in the field coordinates. Simulation waveforms exhibit excellent transient response of the current loops; the dynamics of the direct and quadrature axes are also observed to be decoupled. An experimental setup consisting of IGBT inverters and a TMS320F240 DSP-based digital controller is developed in the laboratory to implement the control algorithms. Relevant experimental waveforms are presented; they are observed to be in good agreement with the simulation results.

Keywords: Rotor induction machine, rotor side control, power applications.

1. Introduction

Wound rotor or slip-ring induction machines are commonly used in large power drives having limited range of operating speeds. The increased cost of a slip-ring machine is justified by the reduced size of the power electronic converter in the rotor circuit. So far, such machines were used as slip power recovery drives with pump or fan type of mechanical loads. However, with the emergence of variable speed constant frequency (VSCF) applications such as wind power generation, there is increased interest towards wound rotor induction machines controlled from the rotor side.

The paper describes the background, concept, simulation and experimental implementation of rotor side control of wound rotor induction machine. A vector control approach using stator flux orientation is employed to decouple the dynamics of the active and reactive current loops. The system is modeled in the field coordinates and simulated to study dynamic and steady-state behaviour. The control algorithm is finally verified on an experimental setup developed for this purpose.

**Author for correspondence.

2. Background

The speed of a cage rotor induction machine is primarily determined by the supply frequency. The short-circuited rotor offers very low resistance and the nominal slip is within 5%. In the case of a wound rotor induction machine it is possible to introduce additional resistance in the rotor circuit and thereby the rotor power loss increases with a corresponding decrease in the shaft output power. For the same load torque this results in an increased slip and a reduction in the shaft speed. Using variable rotor resistance it is, therefore, possible to vary the slip power and hence the rotor speed.[1]

If the slip power is absorbed by an appropriate electrical source instead of being wasted in the resistive elements, the same objective can be achieved. The rotor power, in this case, is regenerated back in electrical form. It is possible to control the amount of power absorbed by the source and hence the shaft speed can be varied. If the source has both sourcing and sinking capabilities, power can be absorbed from or injected into the rotor circuit. The slip can therefore be positive or negative enabling both sub- and supersynchronous operation.

Historically, the controllable electrical source used in the rotor circuit was another auxiliary machine. The slip power was recovered back either in mechanical form (Kramer system) or in electrical form (Scherbius system). With the advent of controllable power devices like silicon-controller rectifiers (SCRs), it is possible to dispense with the additional machines. The variable frequency slip power could be recovered by introducing a phase-controlled converter at the grid interface. Different configurations were proposed by several researchers subsequently.[2–5] In all these schemes, the rotor power can flow in one direction only; so the machine can operate either at sub- or at supersynchronous speeds. However, instead of the dual converter system, use of a cycloconverter in the rotor circuit permits power flow in both directions.[6–9]

3. Rotor side control with back-to-back inverter configuration

Presently, increased attention is being paid to rotor side control of wound rotor induction machine for VSCF wind power generation. Voltage source inverters using IGBTs have become the *de facto* choice for variable speed drives in the 90s. The diode bridge and thyristor inverter combination in the static Scherbius system is replaced by two back-to-back insulated gate bipolar transistor (IGBT) inverters with a capacitive DC link (Fig. 1). Standard three-phase bridge topology is employed for the inverters. With a pulsewidth modulated (PWM) inverter in the rotor circuit, the rotor currents can be controlled in phase, frequency and magnitude. This enables reversible flow of active power in the rotor and the system can operate at sub- and supersynchronous speeds, both in motoring and generating modes. The DC link capacitor acts as a source of reactive power and it is possible to supply the magnetizing current, partially or fully, from the rotor side. The stator side power factor can thus be controlled. Using vector control techniques, the active and reactive powers can be controlled independently and hence fast dynamic performance can also be achieved.

The converter used at the grid interface is termed as the line-side converter or the front-end converter (FEC). Unlike the rotor-side converter, this operates at the grid frequency. Flow of active and reactive powers is controlled by adjusting the phase and amplitude of the inverter

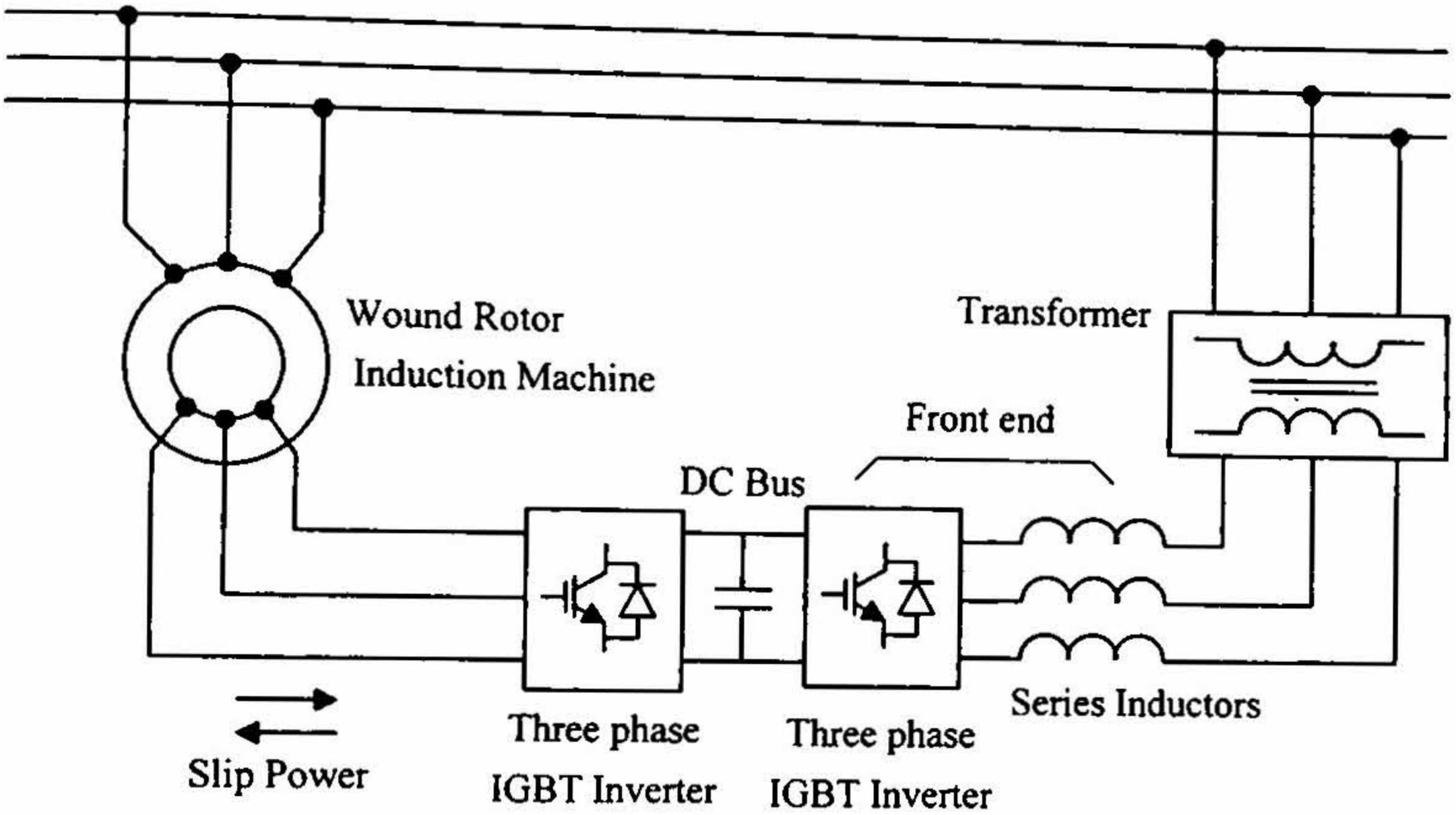

FIG. 1. Rotor side control scheme with back-to-back PWM inverters with capacitive DC link.

terminal voltage with respect to the grid voltage. Active power can flow either to the grid or to the rotor circuit depending on the mode of operation. By controlling the flow of active power, the DC bus voltage is regulated within a small band. Control of reactive power enables unity power factor operation at the grid interface. In fact, the FEC can be operated at a leading power factor, if it is so desired. Since the inverter operates at a high frequency, usually between 1 and 5 kHz, the harmonics in the input current are largely reduced.

It should be noted that since the slip range is limited, the DC bus voltage is lesser in this case when compared to stator side control. A transformer is therefore necessary to match the voltage levels between the grid and the DC side of the FEC.

This arrangement offers enormous flexibility in terms of control of active and reactive powers in variable speed applications. In the following section, the concept of controlling the power flow in the machine by injecting currents in the rotor circuit is explained by deriving suitable phasor diagrams and power flow diagrams.

4. Rotor side control: Modes of operation

The operating region of the system in the torque speed plane is shown in Fig. 2. As stated earlier, the rotor side control strategy is advantageous within a limited slip range. Hence the operating region is spread out on both sides of the synchronous speed (ω_s) implying both sub- and supersynchronous modes of operation. Moreover, the machine can operate in the motoring and generating modes irrespective of the speed. Thus four distinct modes of operation can be achieved through rotor side control corresponding to the four quadrants in the torque speed plane.

In Fig. 2, mode 1 refers to positive torque and subsynchronous speed and is termed as subsynchronous motoring (i.e. normal motoring) operation. Mode 2 corresponds to positive

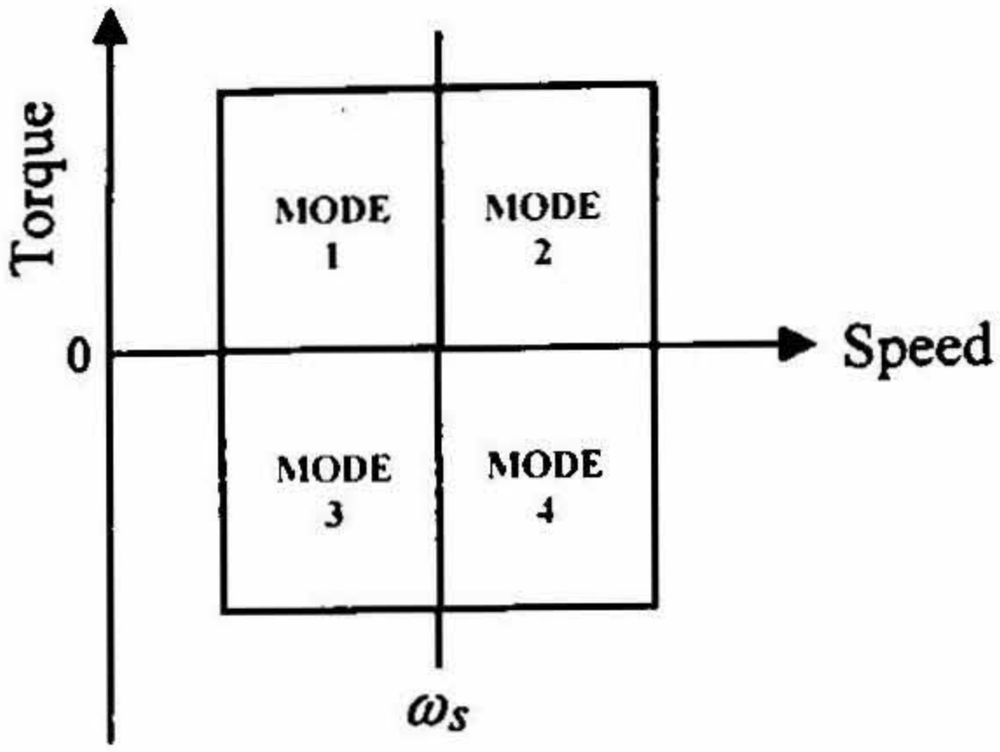

FIG. 2. Operating region of the doubly fed induction machine with rotor side control.

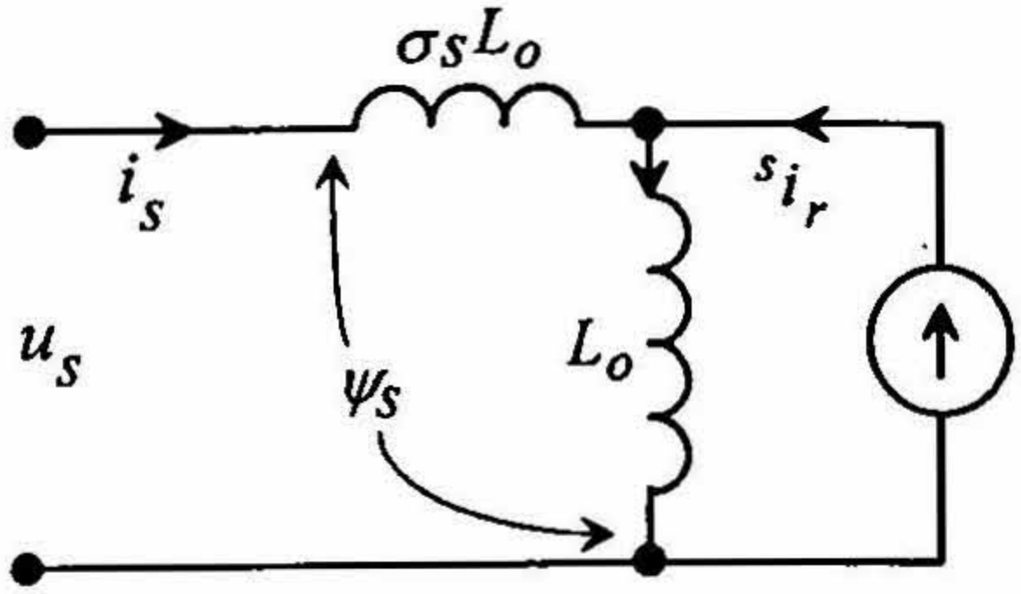

FIG. 3. Approximate equivalent circuit with rotor current control.

torque and supersynchronous speed and is called supersynchronous motoring. Similarly, mode 3 corresponds to subsynchronous generation and mode 4 to supersynchronous generation. The following sections describe how these different modes of operation can be achieved through rotor side control.

4.1. *Mode 1: Subsynchronous motoring*

A simplified equivalent circuit of the doubly fed wound rotor induction machine controlled from the rotor side is shown in Fig. 3. It is assumed that the rotor currents can be injected at any desired phase, frequency and magnitude. Therefore, the rotor circuit can be represented by a controllable current source. The equivalent circuit is drawn in the stator reference frame; hence the rotor current is represented as $^s i_r$. The steady-state phasor diagram and power flow diagram for the subsynchronous motoring mode of operation are shown in Fig. 4.

Neglecting the stator resistance, it may be assumed that the stator flux (ψ_S) remains constant in magnitude and frequency since the stator is connected to the power grid. ψ_S has two components; the stator leakage component and the magnetizing component. The former is due to the stator current alone, while the latter is due to both the stator and rotor currents. An equivalent current (i_{ms}) can be defined in the stator reference frame, which is responsible for the stator flux. This is termed as the stator flux magnetizing current.[10] The direction of ψ_S (which is in phase with i_{ms}) is defined as the d-axis and the direction of the stator voltage, which is at quadrature of ψ_S, is termed as the q-axis. It is possible to resolve i_s and $^s i_r$ along and perpendicular to i_{ms}. (The components of the currents along the d-axis are represented with subscript d, and those along the q-axis with subscript q).

Since ψ_S is constant, it implies that i_{ms} is also constant and equals the sum of i_{sd} and i_{rd}. With current control being exercised in the rotor circuit, an injection of positive i_{rd} will naturally result in a lesser value of i_{sd} being drawn from the stator terminals. The stator power factor is thereby improved. This feature is clearly depicted in Fig. 4(a) and (b). Fig. 4(a) shows i_{ms} being fully supplied from the stator side, as in the case of a cage rotor induction machine, whereas in Fig. 4(b) it is partially supplied from the rotor side and partly from the stator side. It may be noted here that i_{rd} will never be made negative. This would mean that the stator has to supply

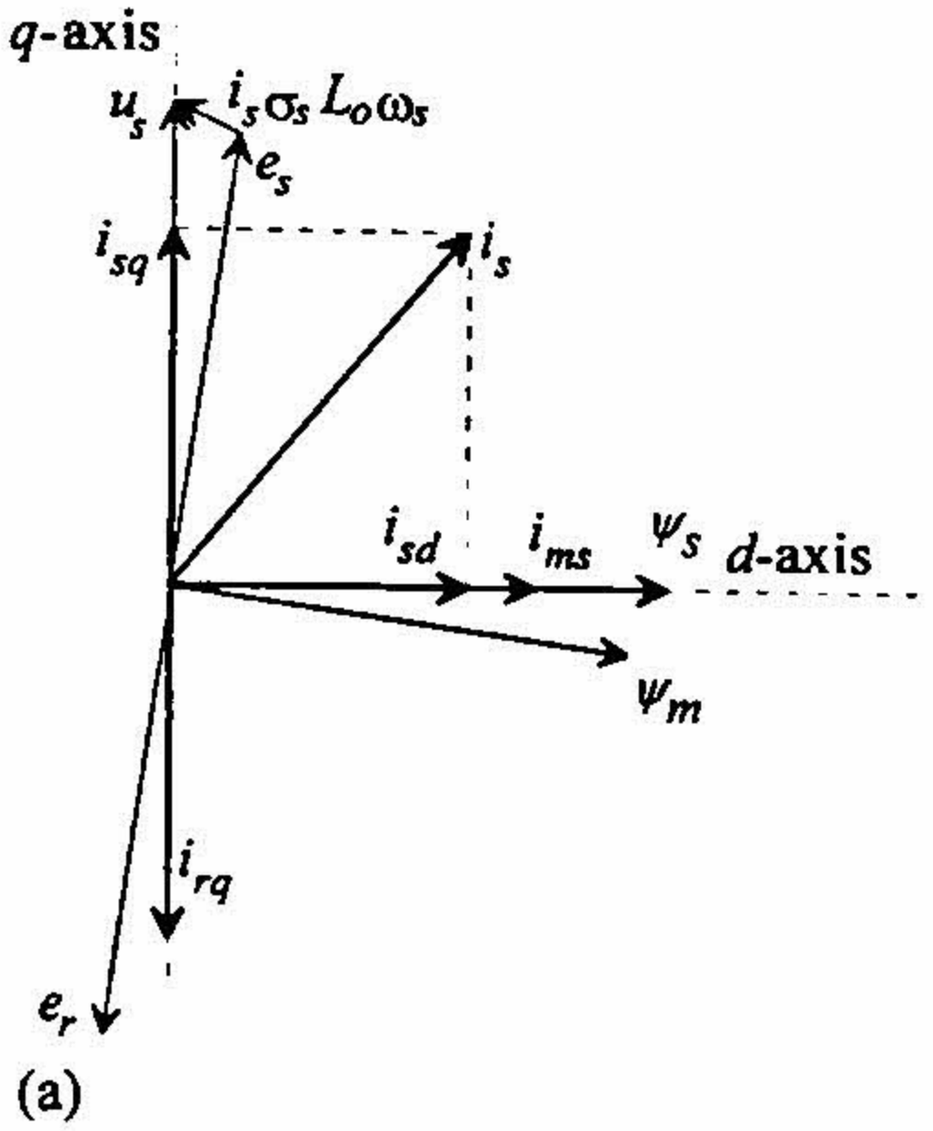

(a)

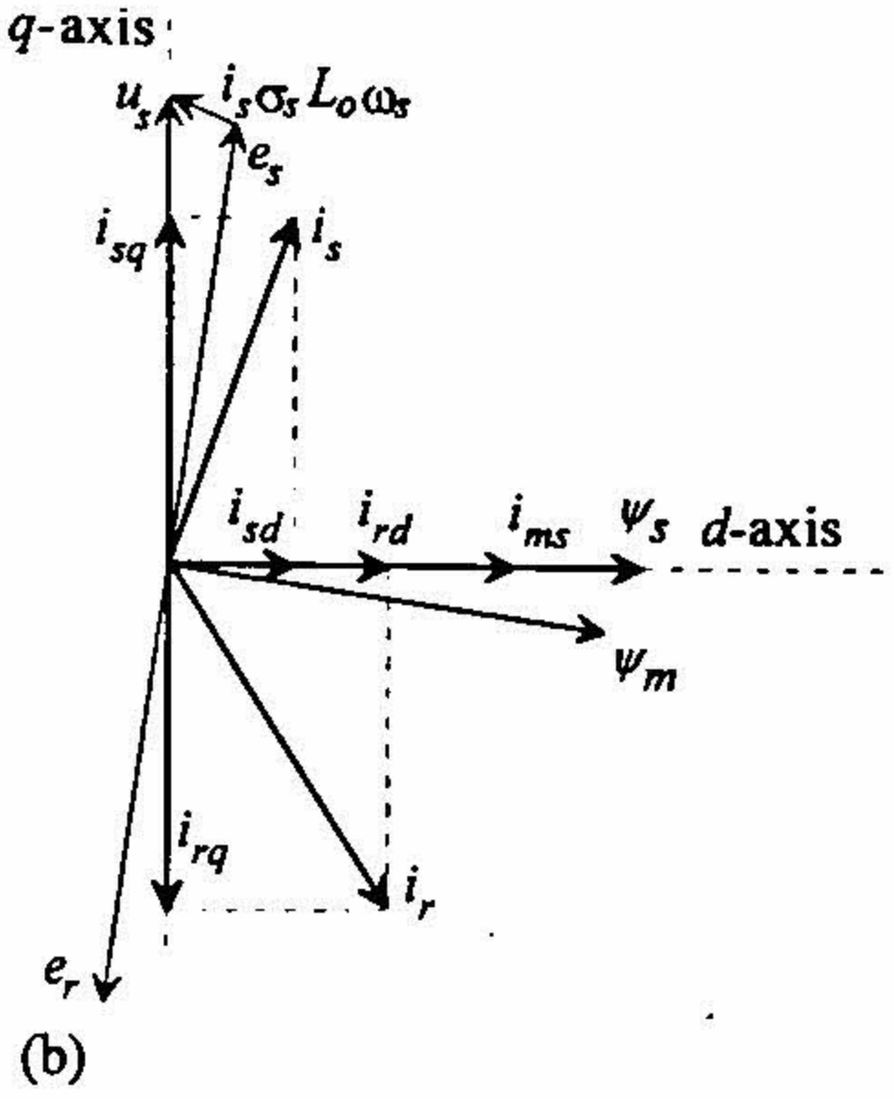

(b)

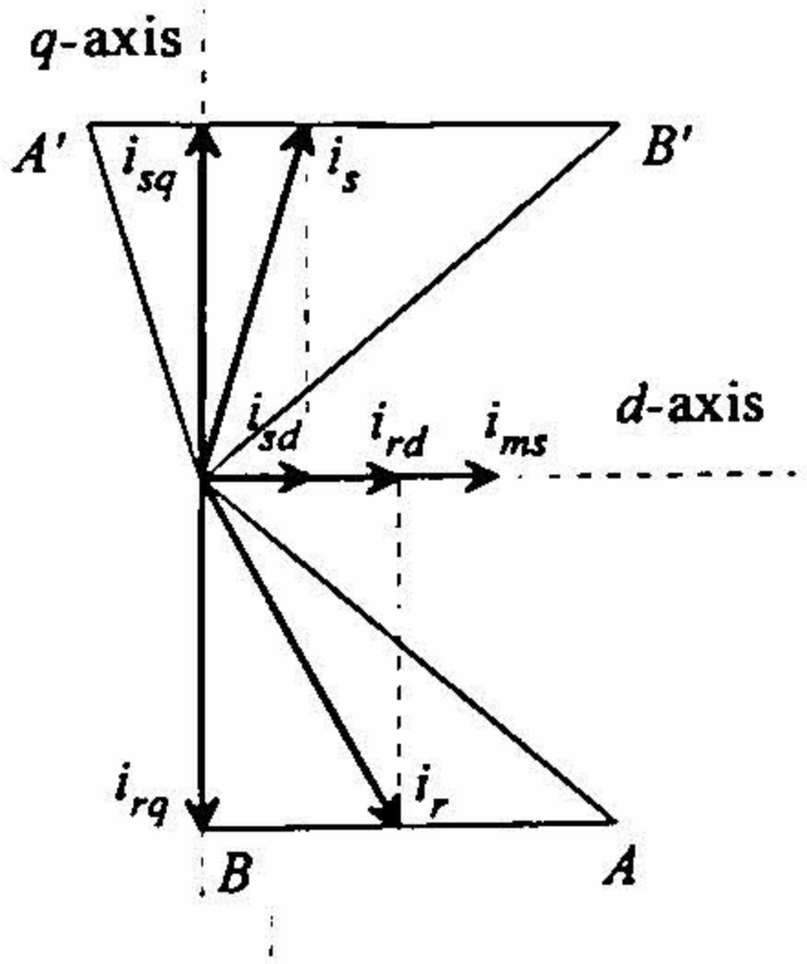

(c)

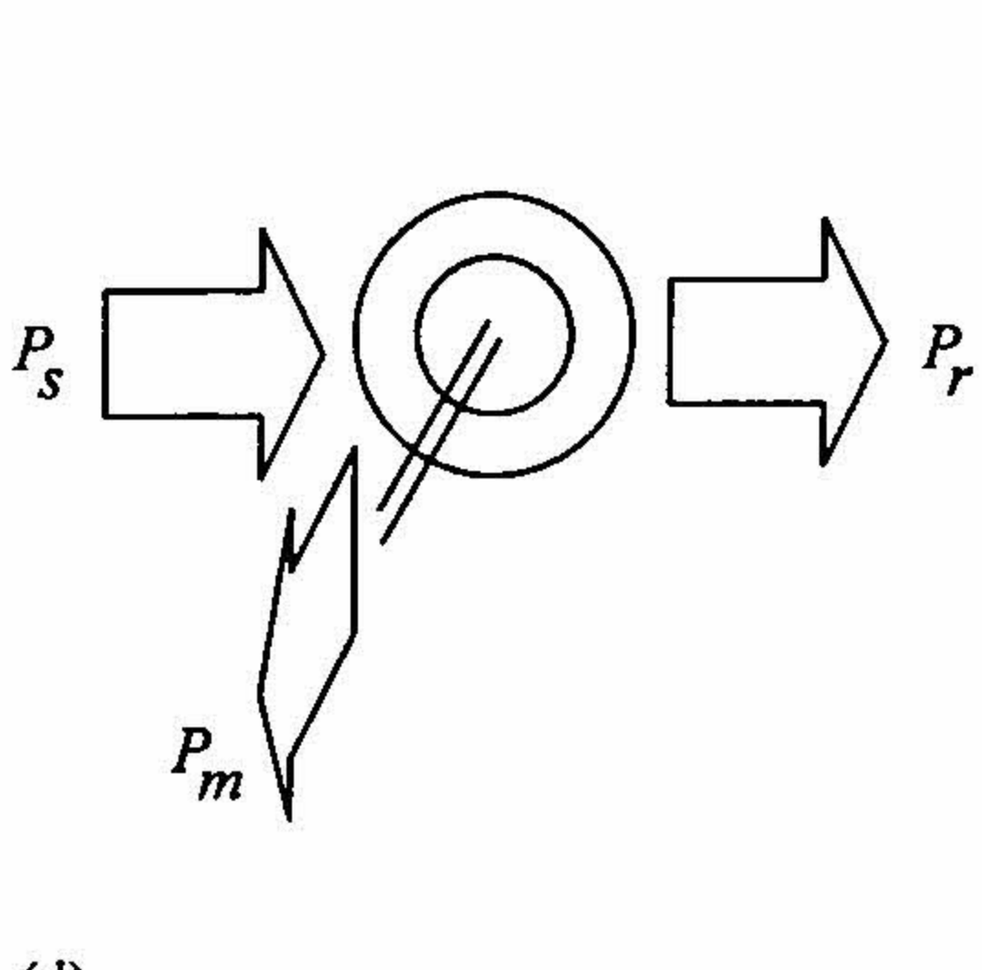

(d)

FIG. 4. (a–c) Phasor diagrams and (d) power flow diagram during subsynchronous motoring.

the magnetizing energy of the machine as well as the reactive energy demand of the rotor circuit bringing down the stator power factor to a very low value.

Along the q-axis, the magnitude of the active component of stator current (i_{sq}) is directly proportional to i_{rq}, but opposite in sign. In fact, the induction machine can be looked upon as a current transformer as far as the active power flow in the stator and rotor circuits is concerned. Hence, to produce a motoring torque (i.e. positive torque), i_{rq} has to be negative. This is evident from Fig. 4; a negative i_{rq} induces a positive i_{sq}, implying flow of active power into the stator circuit. Below the synchronous speed the rotor falls behind the air-gap flux and the rotor-induced emf (e_r) lags the mutual flux (ψ_m) by 90° as shown in Fig. 4(a) and (b).

The locus of i_s and i_r for constant active power flow is shown in Fig. 4(c) . As the tip of the rotor current phasor is moved from B to A, the stator current phasor locus moves in the opposite direction from B' to A'. From this phasor diagram it may be appreciated that some amount of reactive power can as well be delivered to the source from the stator side, when the reactive power supplied from the rotor side is more than the machine requirement. This is, however, possible when the active load demand is low and there is adequate current margin in the rotor coils. In order to utilize the copper in the stator and rotor circuits effectively, it is advisable to divide the reactive power demand between the two ports.

Under the condition of subsynchronous motoring the stator voltage phasor (u_s) leads the air-gap voltage $e_s(=-e_r)$ under all conditions of load which indicates power flowing into the stator. Also the rotor current (i_r) makes an angle less than 90° with e_r, the rotor-induced emf, implying that active power is being extracted from the rotor circuit. This rotor power, or the slip power, is recovered from the rotor circuit and fed back to the mains, thereby increasing system efficiency. The mechanical power output is roughly the difference between the stator and rotor powers (Fig. 4(d)).

4.2. *Mode 2: Supersynchronous motoring*

With i_{rq} remaining negative if the machine runs above synchronous speed, it enters the supersynchronous motoring mode of operation. The rotor now moves ahead of the air-gap flux (ψ_m) and, therefore, e_r leads ψ_m by 90°. The phase relations between the stator and rotor currents remain as in mode 1; only the direction of rotor power reverses as i_r now makes an angle more than 90° with e_r (Fig. 5).

It may be noted that in this mode of operation, if the stator input power is 1 p.u. and the motor is running at a slip of s p.u., the mechanical output that can be obtained is $(1 + s)$ p.u. which is more than the rating of the machine.

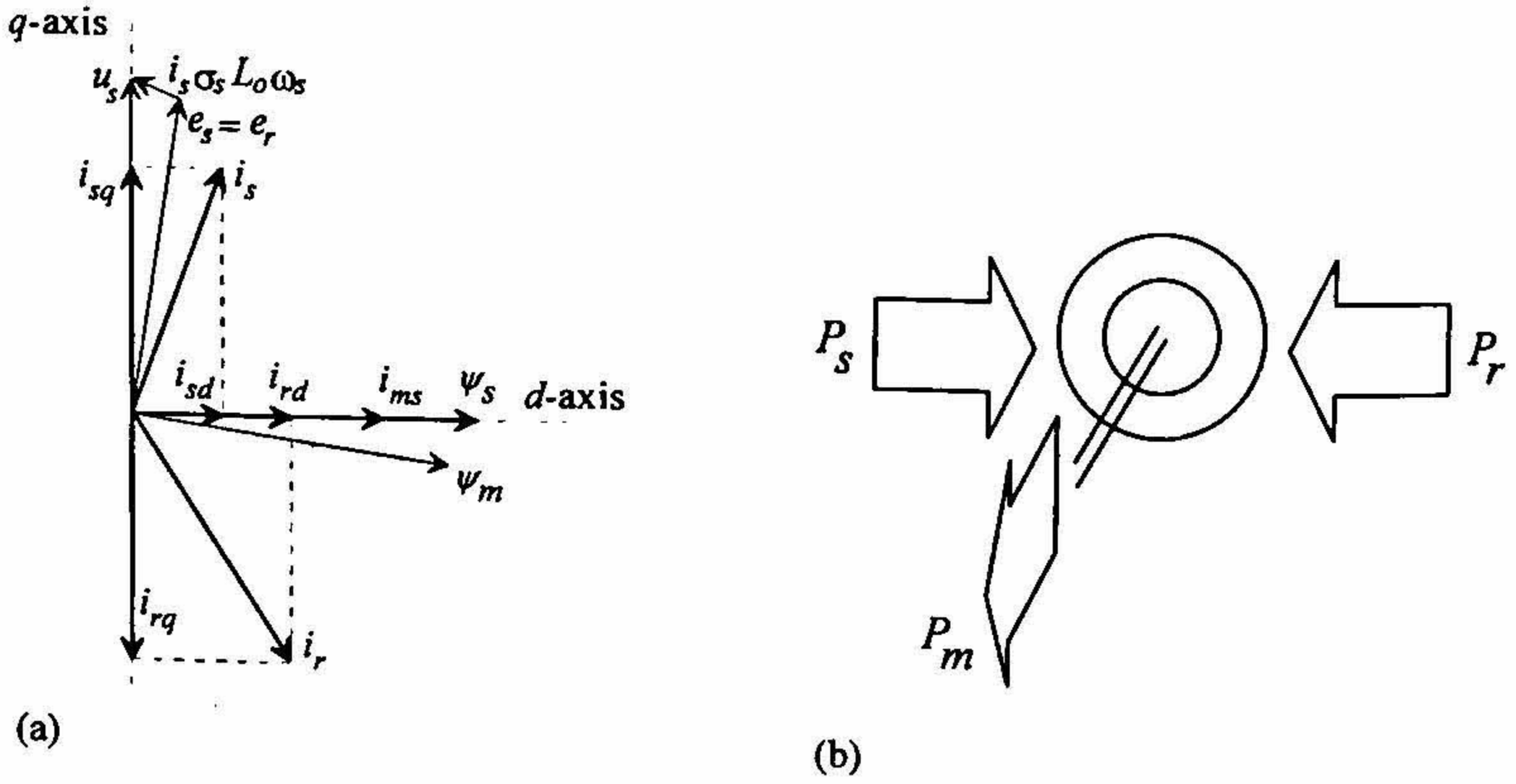

FIG. 5. (a) Phasor and (b) power flow diagrams during supersynchronous motoring.

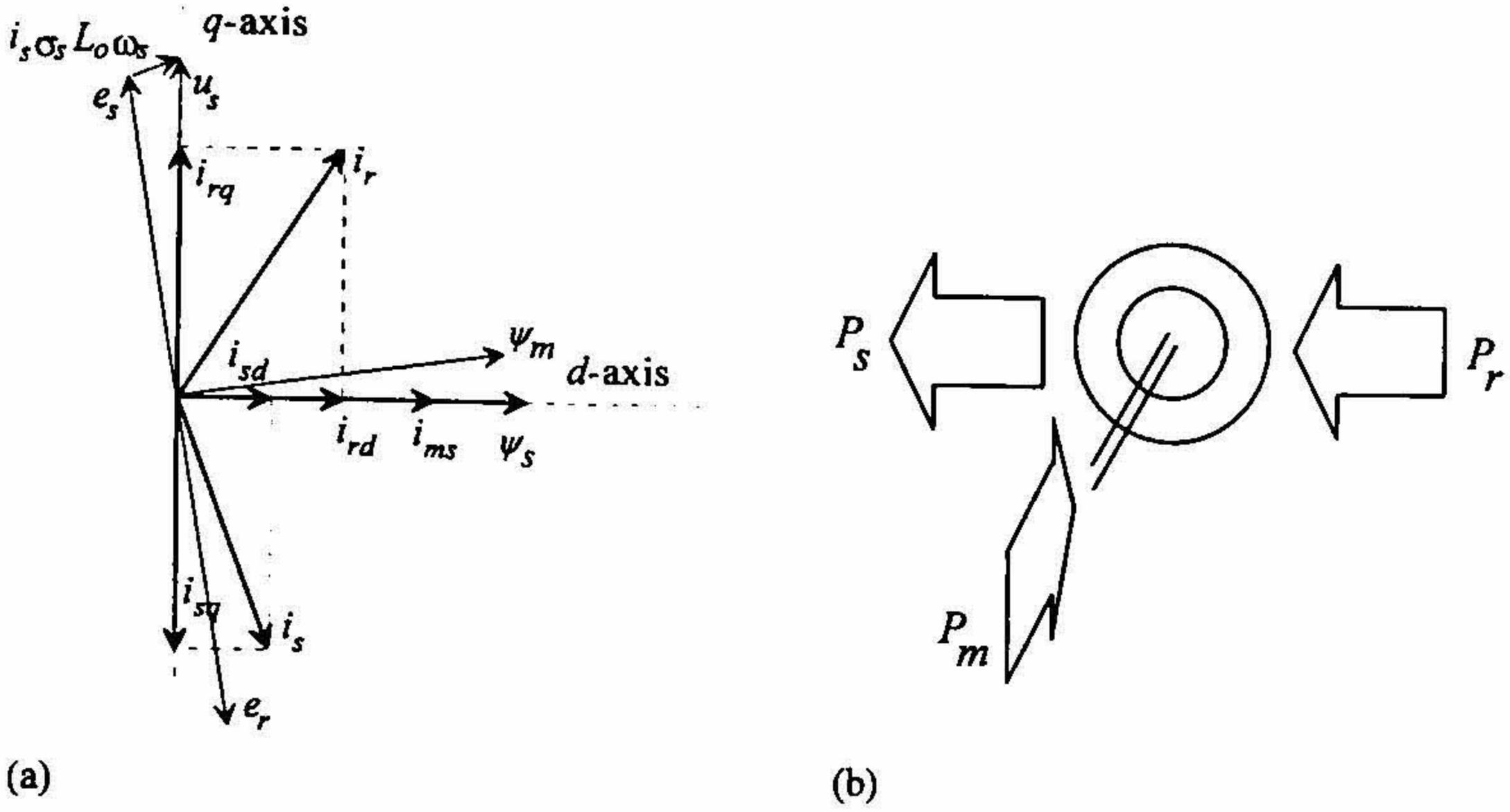

FIG. 6. (a) Phasor and (b) power flow diagrams during subsynchronous generation.

4.3. *Mode 3: Subsynchronous generation*

If a positive i_{rq} is injected into the rotor circuit, i_{sq} changes direction and becomes negative. Therefore, the active power flow into the stator becomes negative indicating that the machine is generating. This can also be appreciated from the fact that the stator terminal voltage vector (u_s) now lags the stator-induced emf. The phase angle between i_r and e_r exceeds 90°, implying that power is fed into the rotor circuit. The power flow and phasor diagrams are given in Fig. 6.

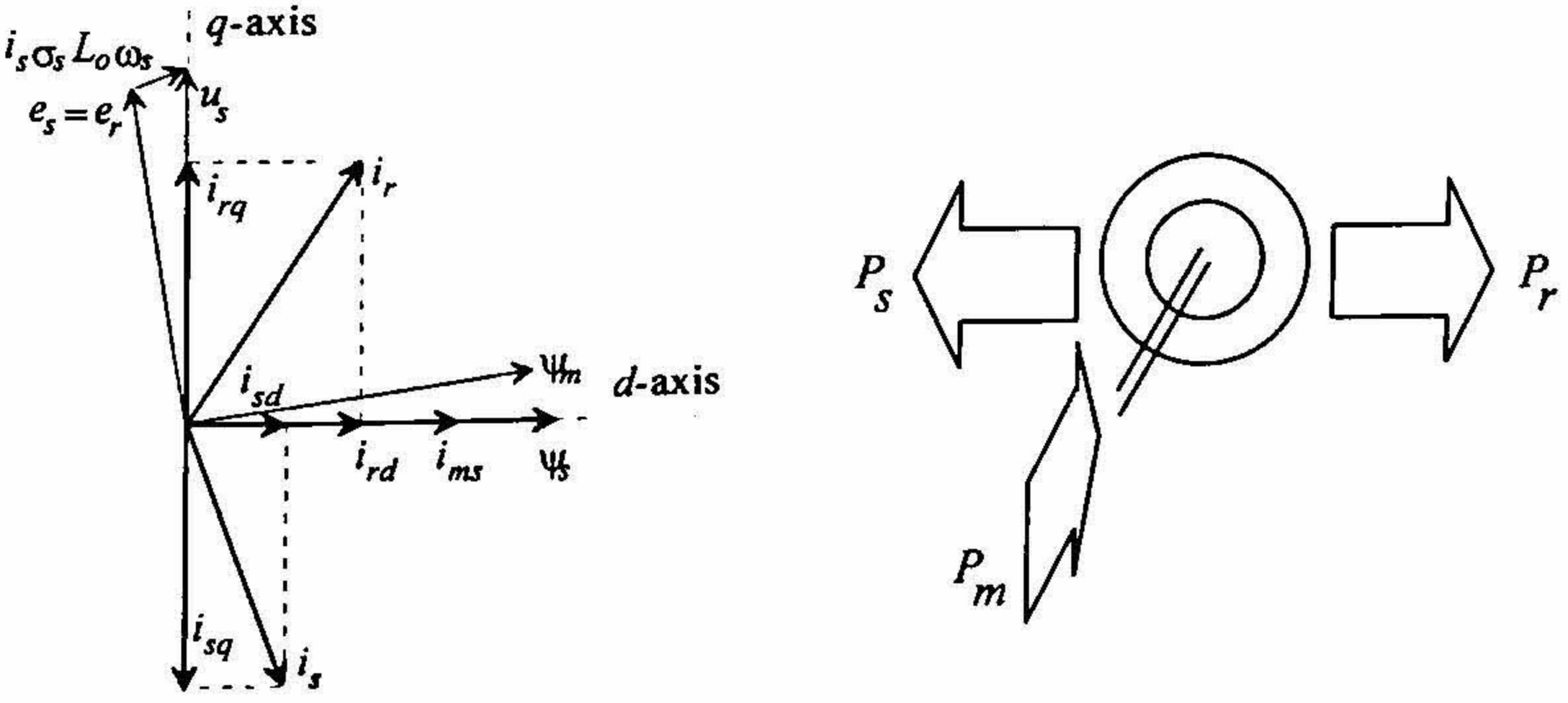

FIG. 7. (a) Phasor and (b) power flow diagrams during supersynchronous generation.

4.4. *Mode 4: Supersynchronous generation*

With i_{rq} remaining positive, the machine can go over to the supersynchronous generating mode. As far as the stator circuit is concerned everything remains the same as in mode 3; only the rotor power flow changes its direction. With the rotor-induced emf e_r leading the air-gap flux, the angle between i_r and e_r becomes less than 90° indicating power flow out of the rotor. It is interesting to note that in supersynchronous generation mode the shaft power is recovered from both the stator and the rotor ends. Therefore, if 1 p.u. power is extracted from the stator, while the machine is running at a slip s, the total power generated will be $(1 + s)$ p.u. Hence in the supersynchronous generation mode it is actually possible to generate power that is more than the rating of the machine (Fig. 7).

5. Decoupled control of active and reactive power through field-oriented control

In order to control the rotor currents in the desired manner, field-oriented control is employed. Stator flux-oriented control of doubly fed wound rotor induction machine has been described by Leonhard[10] and Vas.[11] Leonhard's approach of field orientation in the stator flux reference frame became popular because of its close resemblance to rotor-flux orientation in cage rotor machines. However, contrary to the cage rotor induction machine, there is an uncontrolled voltage source connected to the stator of a doubly fed wound rotor induction machine. This acts as a disturbance variable in the plant model. The current controller, therefore, needs to be designed in such a way that the effect of the disturbance terms are nullified.

With reference to Fig. 8, the complete set of equations that describe the machine dynamics in the field coordinates can be derived as

$$T_s \frac{di_{ms}}{dt} + i_{ms} = \frac{1+\sigma_s}{R_s} u_{sd} + i_{rd} \tag{1}$$

$$\frac{d\mu}{dt} = \omega_{ms} = \frac{1}{T_s i_{ms}} \left[\frac{1+\sigma_s}{R_s} u_{sq} + i_{rq} \right] \tag{2}$$

$$J \frac{d\omega}{dt} = -\frac{2}{3} \frac{P}{2} \frac{L_0}{1+\sigma_s} i_{ms} i_{rq} - m_l \tag{3}$$

$$\frac{d\varepsilon}{dt} = \frac{P}{2} \omega = \omega_e. \tag{4}$$

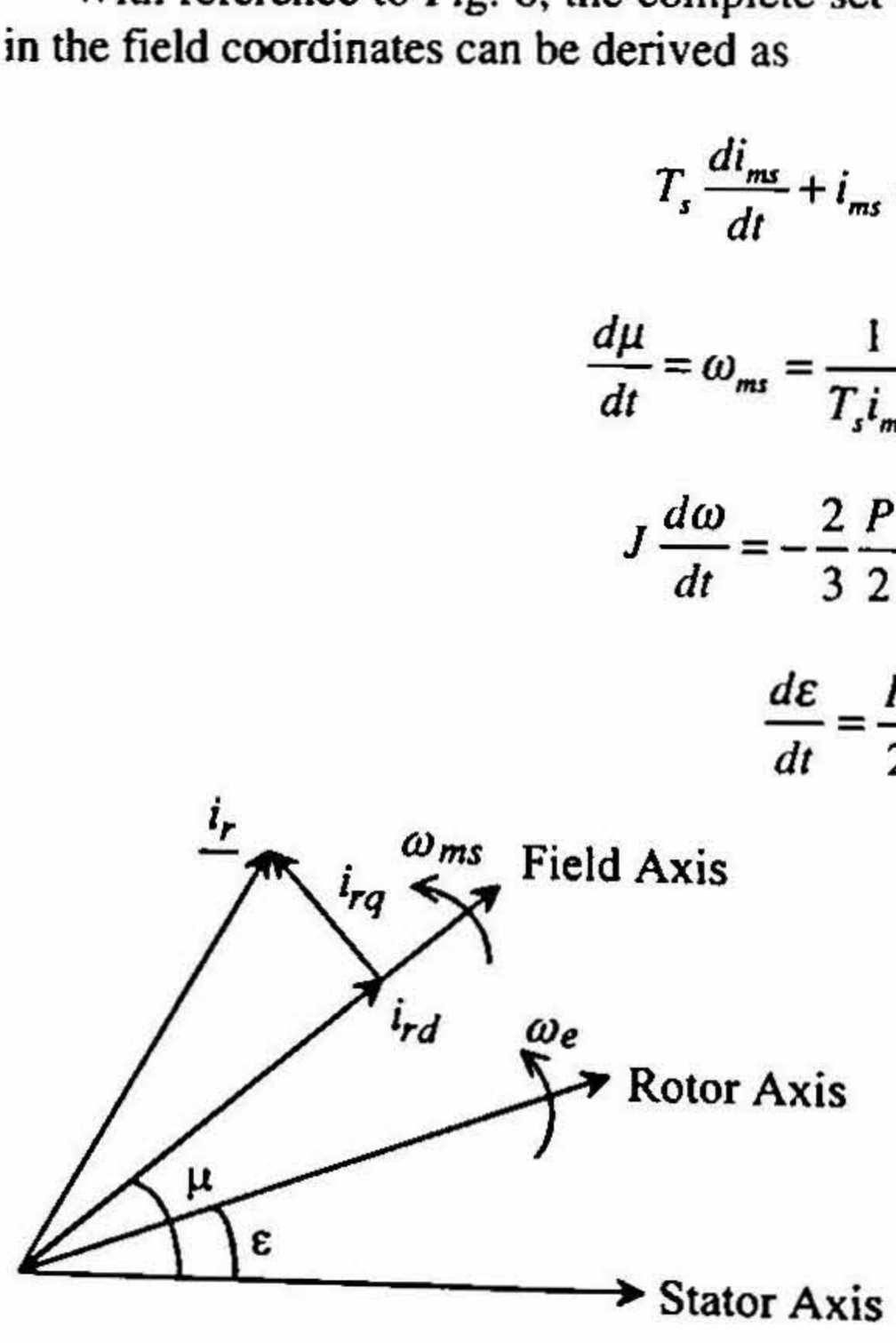

FIG. 8. Angular relations of current vectors for doubly fed induction machine.

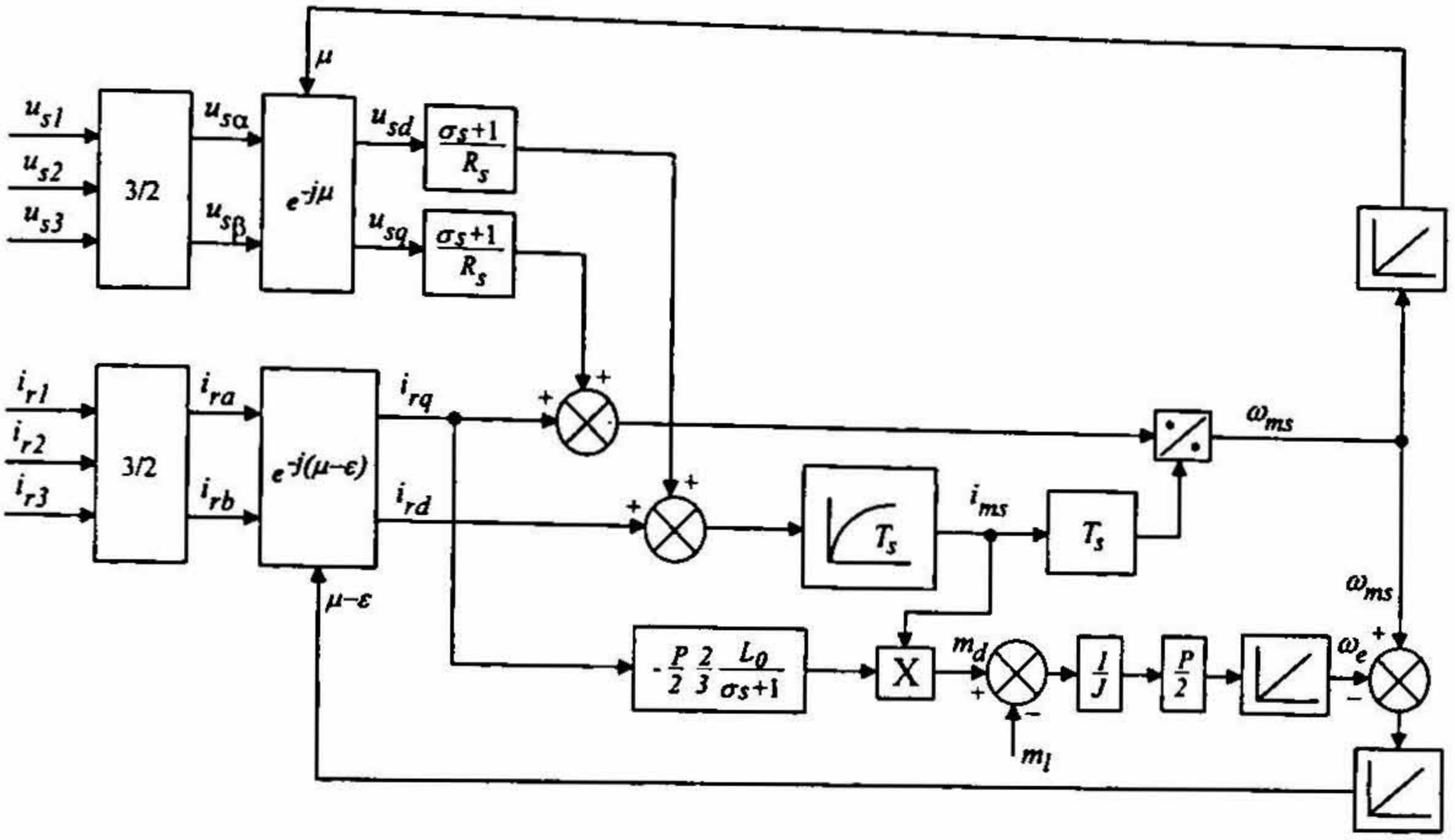

FIG. 9. Block diagram of the doubly fed wound rotor induction machine model in the field coordinates.

The simulation block diagram of the doubly fed wound rotor induction machine modelled in the field coordinates is given in Fig. 9. The inputs to the system are the stator voltage and the rotor currents. It is assumed that there is a controlled current source in the rotor circuit which is capable of injecting currents at appropriate phase, frequency and magnitude. The rotor currents are first transformed to the stator reference frame using the operator $e^{j\epsilon}$. Subsequently, the stator voltages and rotor currents (in the stator reference frame) are transformed to the field coordinates by multiplying with $e^{-j\mu}$. The angle μ is derived by solving the q-axis equation (eqn (2)). The magnitude of i_{ms} is computed using the d-axis equation (eqn (1)). It may be noted that the alternating quantities in the stationary coordinates, when transformed to the field coordinates, appear as DC quantities.

For designing the rotor current controller the rotor voltage equation has to be considered.

$$\sigma T_r \frac{di_{rd}}{dt} + i_{rd} = \frac{u_{rd}}{R_r} + (\omega_{ms} - \omega_e)\sigma T_r i_{rq} - (1-\sigma)T_r \frac{di_{ms}}{dt} \tag{5}$$

$$\sigma T_r \frac{di_{rq}}{dt} + i_{rq} = \frac{u_{rq}}{R_r} - (\omega_{ms} - \omega_e)\sigma T_r i_{rd} - (\omega_{ms} - \omega_e)(1-\sigma)T_r i_{ms}. \tag{6}$$

These equations represent the dynamics of the rotor currents in the field coordinate system. It is observed that due to the presence of the rotational emf terms, there is some amount of cross coupling between the d and q axes. However, the current loop dynamics in the two axes can be made independent of each other by compensating for these cross-coupling terms.

It is obvious that if the rotor current needs to be controlled in the field coordinates, two independent controllers are needed; one each for the d- and q-axes. The design method is the

same for both; only the feedforward terms differ in each case. The design of a proportional (P) controller and a proportional-integral (PI) controller are presented here.

5.1. *Proportional controller*

Let the desired current loop dynamics in the d-axis be given by

$$T_{ir}\frac{di_{rd}}{dt}+i_{rd}=\frac{i_{rd}^{*}}{K_{ir}} \tag{7}$$

where T_{ir} is the desired current-loop time constant and K_{ir} the current sensor gain.

The task is now to find out the d-axis component of the instantaneous inverter terminal voltage required to produce the current dynamics given by eqn (7).

Substituting for di_{rd}/dt from eqn (7) in eqn (5) gives

$$u_{rd}=\frac{\sigma L_r}{T_{ir}K_{ir}}\left(i_{rd}^{*}-K_{ir}i_{rd}\right)+R_r i_{rd}+(1-\sigma)L_r\frac{di_{ms}}{dt}-(\omega_{ms}-\omega_e)\sigma L_r i_{rq}. \tag{8}$$

The inverter can be modelled as a gain block G_r. For sine-triangle modulation the inverter gain depends on the DC bus voltage u_{dc} and the peak of the triangle u_{tri}.

$$G_r=\frac{u_{dc}}{2*u_{tri}}. \tag{9}$$

In order to make the inverter gain constant, the peak of the carrier triangular waveform u_{tri} is made proportional to u_{dc}.

Therefore, the reference for the d-axis component of the rotor voltage is given by

$$u_{rd}^{*}=\frac{u_{rd}}{G_r}=\frac{\sigma L_r}{T_{ir}K_{ir}G_r}(i_{rd}^{*}-K_{ir}i_{rd})+\frac{R_r}{G_r}i_{rd}+\frac{(1-\sigma)L_r}{G_r}\frac{di_{ms}}{dt}-\frac{(\omega_{ms}-\omega_e)\sigma L_r}{G_r}i_{rq}. \tag{10}$$

Assuming same current loop dynamics for the q-axis, the reference for the q-axis component of the rotor voltage can be expressed as

$$u_{rq}^{*}=\frac{u_{rq}}{G_r}=\frac{\sigma L_r}{T_{ir}K_{ir}G_r}(i_{rq}^{*}-K_{ir}i_{rq})+\frac{R_r}{G_r}i_{rq}+\frac{(\omega_{ms}-\omega_e)(1-\sigma)L_r}{G_r}i_{ms}+\frac{(\omega_{ms}-\omega_e)\sigma L_r}{G_r}i_{rd}. \tag{11}$$

If the impressed rotor voltages are in accordance with eqns (10) and (11), the field and quadrature axes rotor currents can be controlled independently. The rotor current controller, therefore, does not contribute significantly to the dynamics of the system. It only ensures that the rotor currents track the reference signals produced by the outer loops. It may be appreciated that the current loop dynamics can be made much faster than the rotor time constant. However, a practical limitation to the bandwidth of the current controller is imposed by the switching

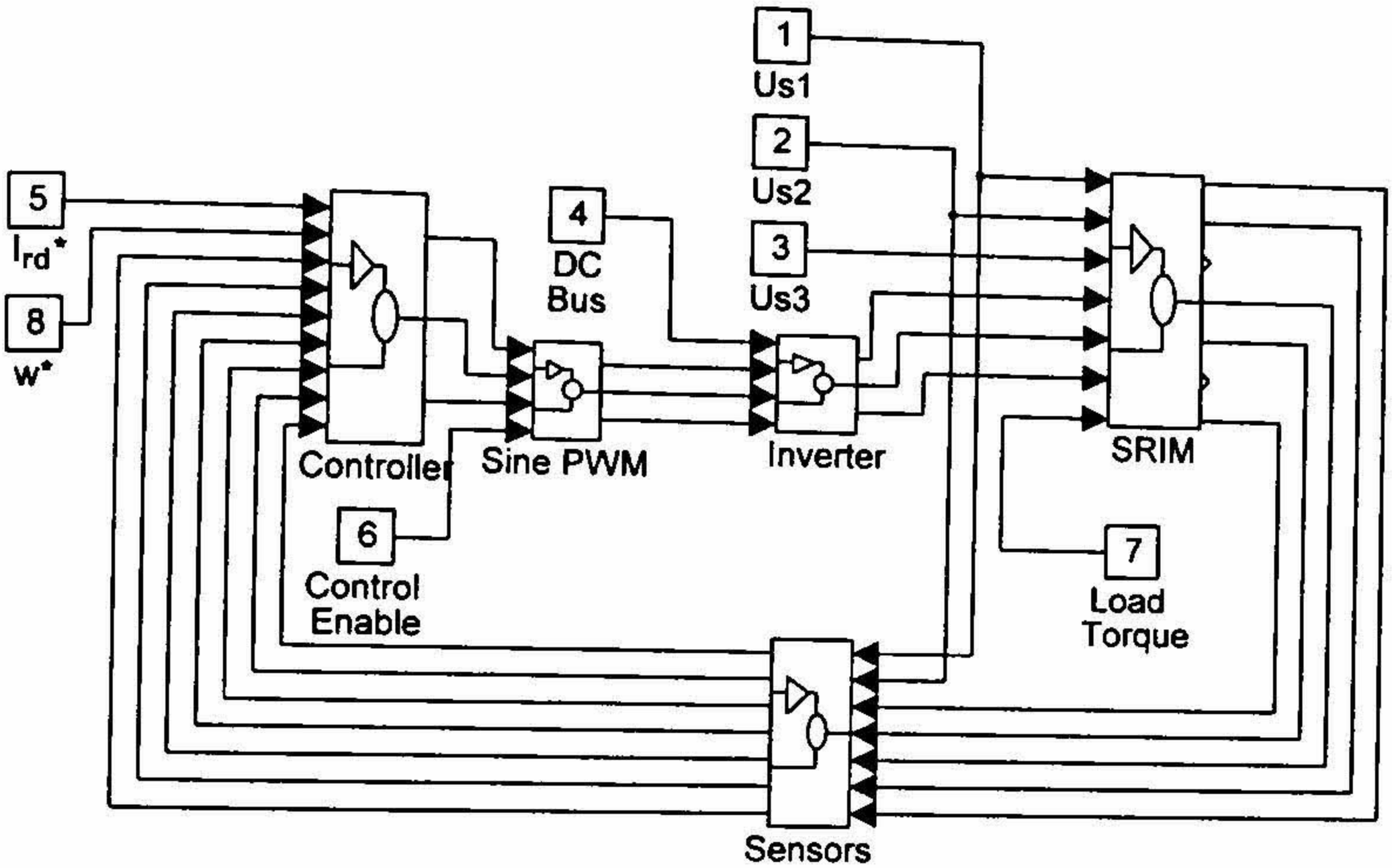

FIG. 10. SIMULINK block diagram of a speed-controlled drive using doubly fed SRIM.

frequency. Since the controller is designed in the field coordinates, all the quantities are DC and implementation of the controller becomes simpler.

5.2. *Proportional integral controller*

In the proportional controller, the steady-state error in the rotor currents will depend on the accuracy of computation of the feedforward terms. Any error in the compensation terms would result in slight modification of the dynamic response. In the practical implementation, it is extremely difficult to perfectly nullify the disturbance terms owing to measurement and computational errors. Therefore, a proportional integral controller needs to be incorporated. This is particularly important when the machine is run in the torque control mode without any outer speed loop. The plant is modelled as a first-order lag system having a time constant of σT_r with the two rotational emfs as disturbance inputs. These two terms are cancelled through feedforward compensation as before. In the controller, the PI time constant is made also equal to σT_r, so that the dynamics of the system is decided by the proportional gain. The choice of proportional gain follows from the equation $K_{pir} = \left(\frac{\sigma T_r}{T_{ir}}\right) R_r$, where T_{ir} is the desired effective time constant of the current loop.

6. Simulation

The entire system is simulated on the MATLAB-SIMULINK platform. The simulation model comprises different functional modules or subsystems. Each of these modules in turn has several levels of subsystems which are developed using the standard SIMULINK library.

A speed-controlled drive using grid-connected doubly fed SRIM is simulated (Fig. 10). Stator flux orientation, as discussed in the earlier sections, is employed. The d- and q-axes current controllers are designed in the field reference frame. For the speed loop, a PI controller is employed which generates the q-axis/active current reference i_{rq}^*. The d-axis reference i_{rd}^* is set in open loop. The machine parameters, sensor gains and controller gains are given in Appendix. The results are presented in unit terms for the sake of uniformity.

The speed response of the drive under no load is given in Fig. 11(a). The motor is started DOL with the rotor shorted. At $t = 0.25$ s, the rotor side control is released with a speed reference $\omega^* = 0.75$ p.u. At $t = 1.25$ s, the speed reference is given a step change from 0.75 to 1.25 p.u. The corresponding motor torque and i_{rq} are given in Figs 11(b) and (c), respectively. The speed controller time constant is set to 100 ms. At $t = 1.75$ s, i_{rd}^* is given a step change to 0.75 p.u. This results in transfer of the reactive power from the stator to the rotor side. However, a change in i_{rd} does not affect i_{rq}, as can be seen from these plots.

The dynamic response of the current loops is given in Figs 12 and 13. The q-axis current loop time constant is designed for 1 ms and the d-axis loop time constant for 4 ms. (The d-axis reference is not required to be varied dynamically; so the dynamic response of i_{rd} need not be very fast). The actual stator and rotor currents in the stator reference frame are also shown. In

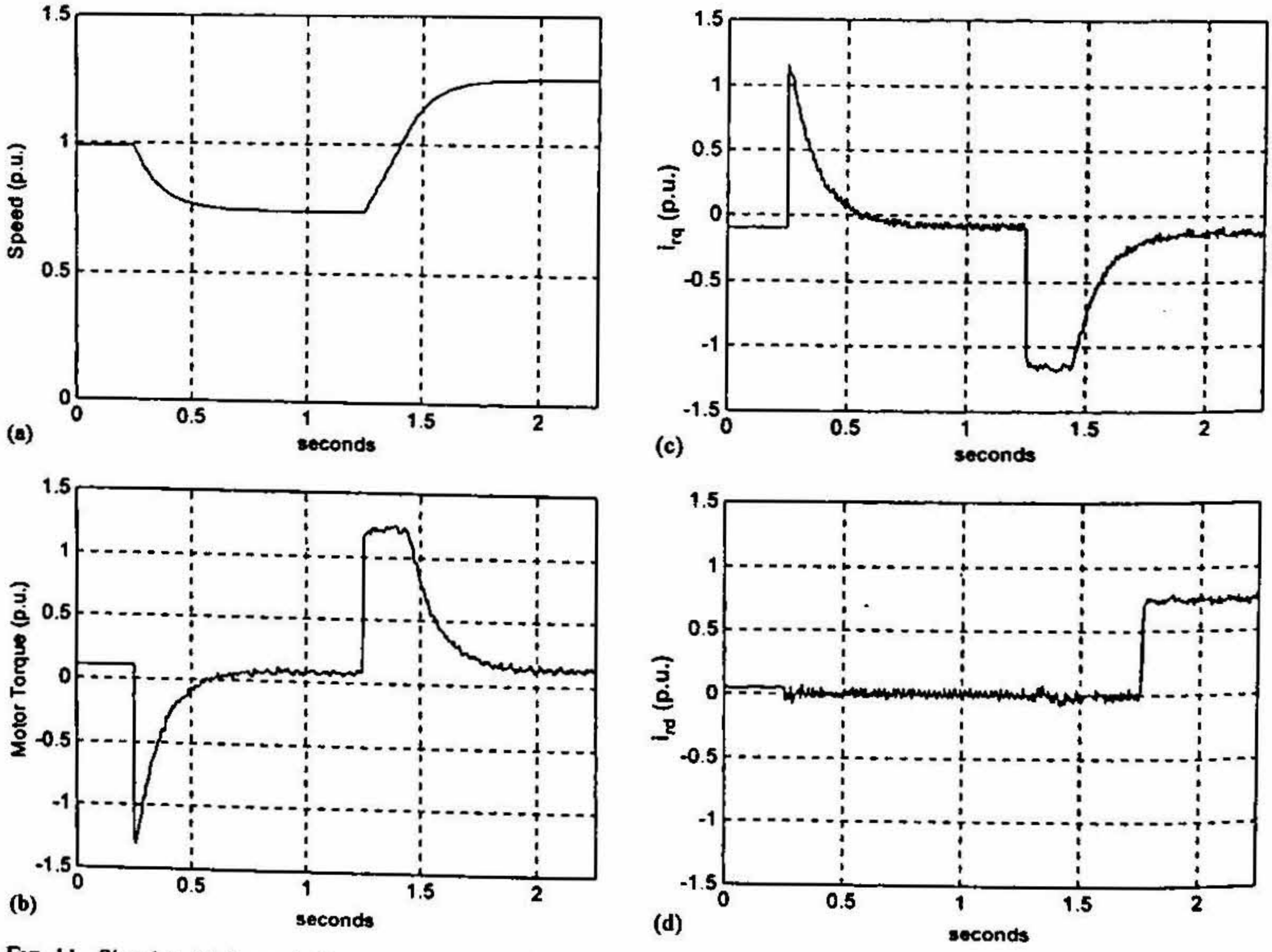

FIG. 11. Simulated (a) speed, (b) torque, (c) i_{rq} and (d) i_{rd} response of the speed-controlled grid-connected SRIM drive.

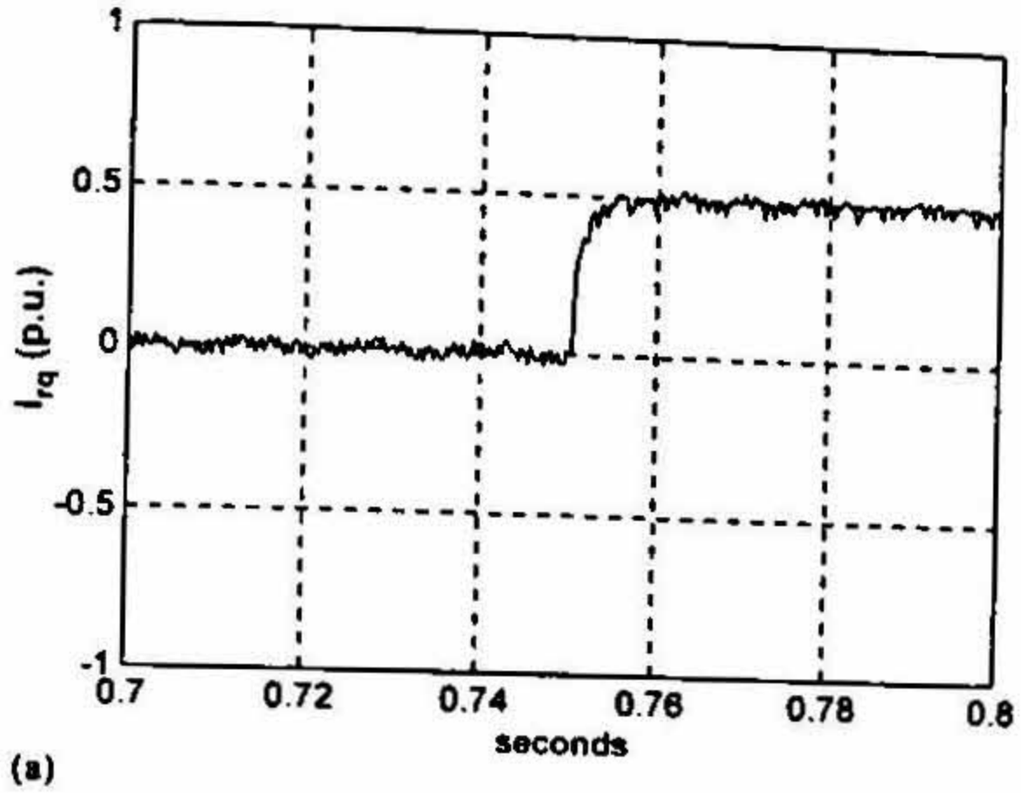

(a)

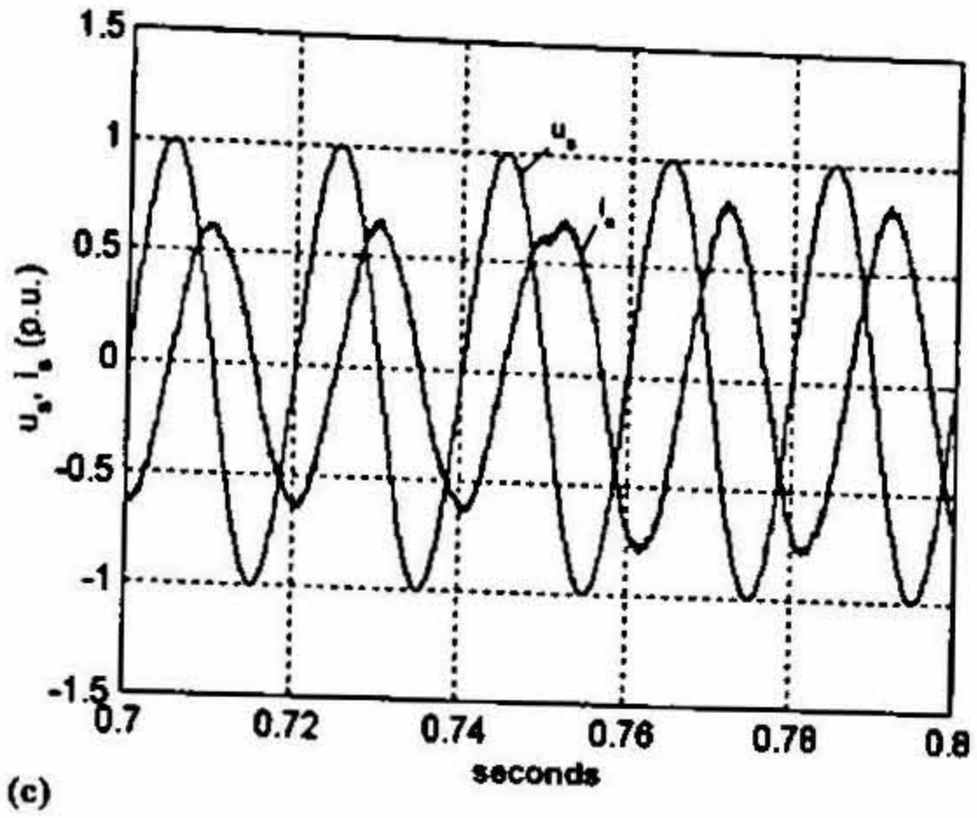

(c)

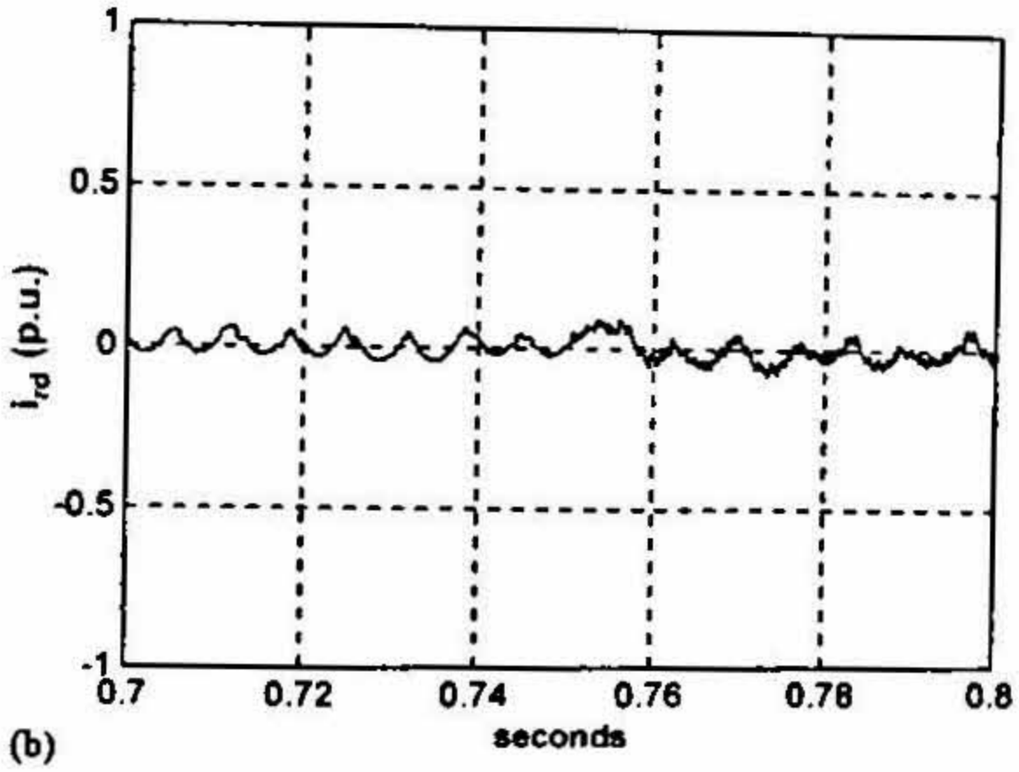

(b)

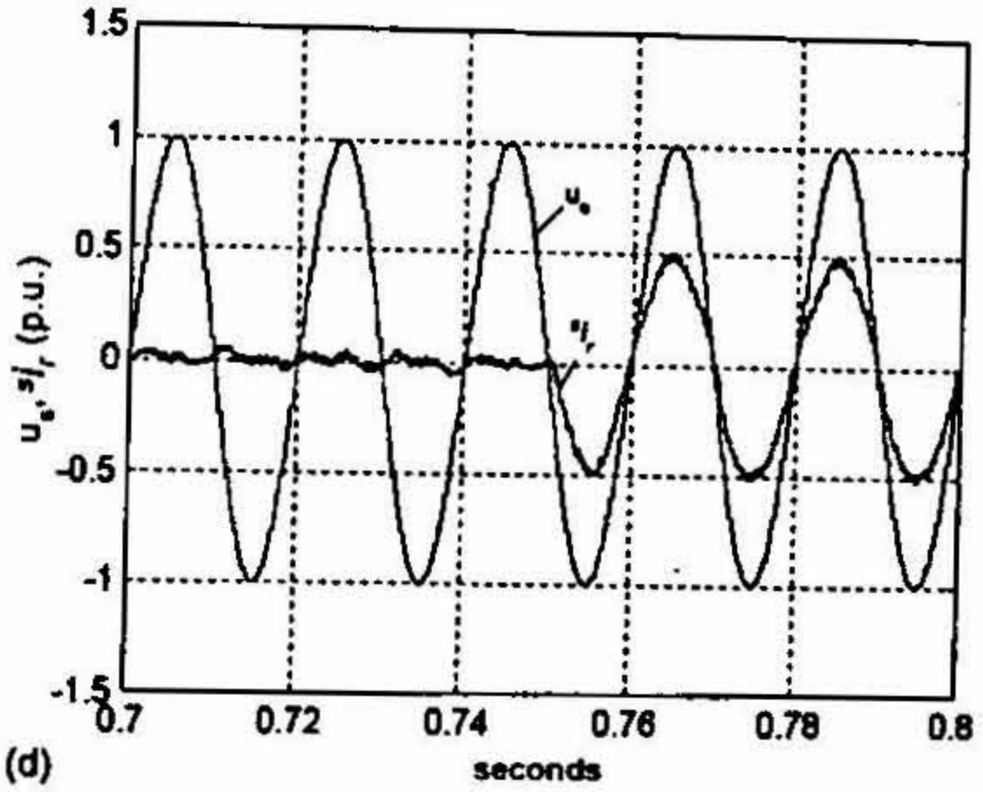

(d)

FIG. 12. Simulated step response of (a) i_{rq}, (b) i_{rd}, (c) i_s along with u_s and (d) ^si_r along with u_s for the grid-connected SRIM.

Fig. 12, i_{rd} is zero, so the stator supplies the reactive power and the rotor power factor is unity. In Fig. 13, the reactive power is transferred from the stator to the rotor side, resulting in an improvement in the stator power factor.

The transition through synchronous speed is shown in the plots of Fig. 14(a) through (d). With an initial speed of 0.6 p.u., the simulation is run with $i_{rq}^* = 0.5$ p.u. and a load torque of –0.88 p.u. (i.e. driving torque). Therefore, the stator power remains constant, while the rotor power goes from positive to negative. The transition of the rotor phase current through synchronous speed is also shown.

7. Experimental implementation

A major emphasis of the present work is to develop a generalized hardware platform for high-performance AC drives. The system organization for rotor side control of doubly fed wound rotor induction machine presents a versatile case where both the machine and line side converters are necessary. In order to demonstrate the application of such a system to wind power generation, the wind turbine characteristics also need to be simulated with a DC drive. The organization of the experimental set-up is schematically shown in Fig. 15.

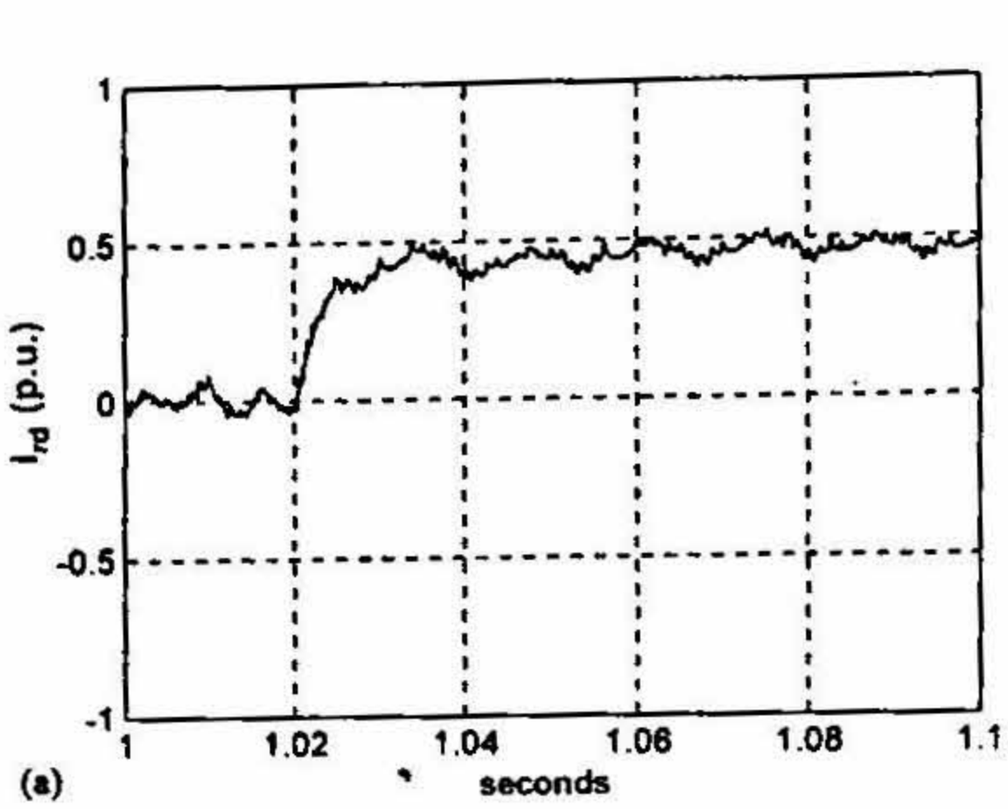

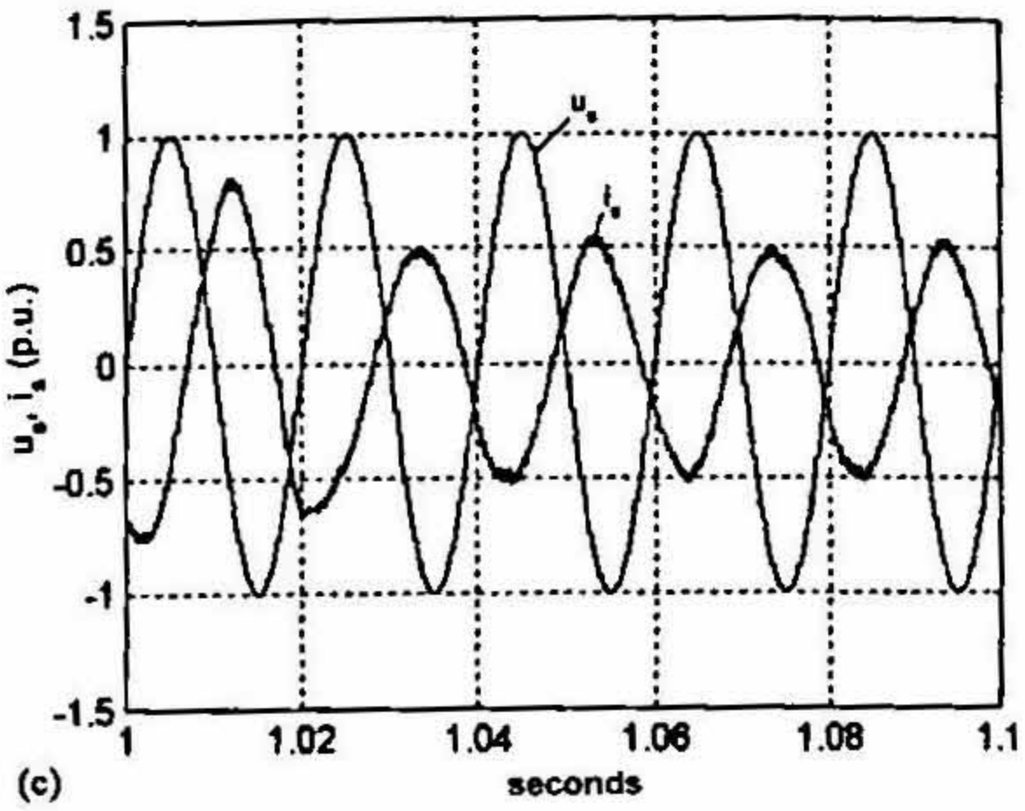

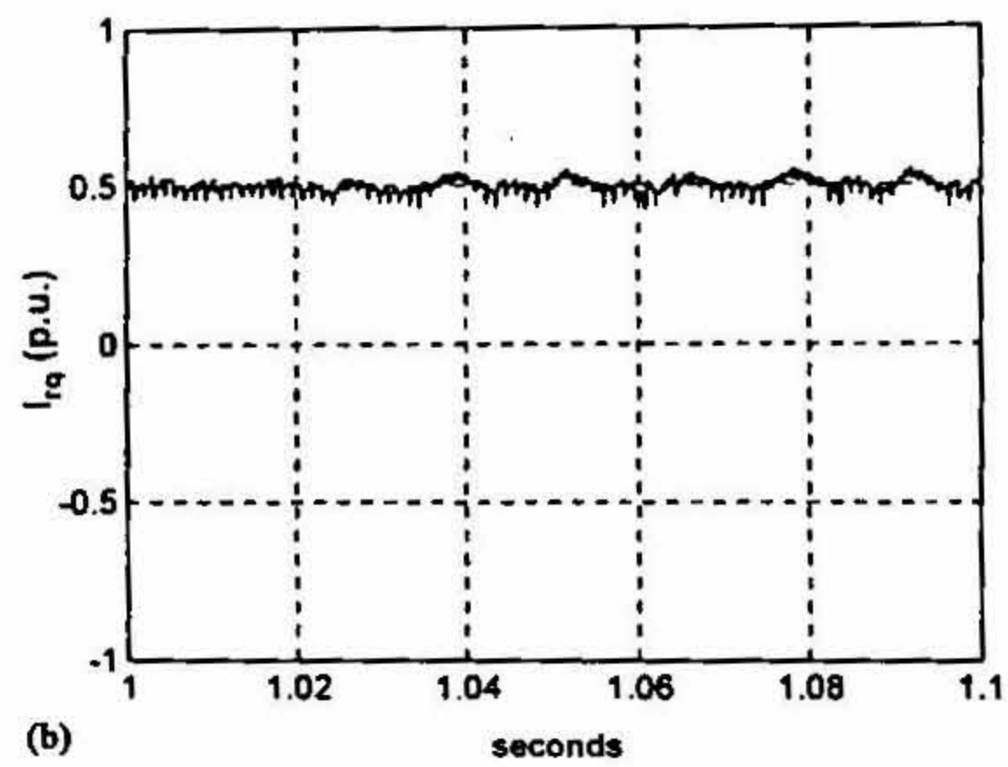

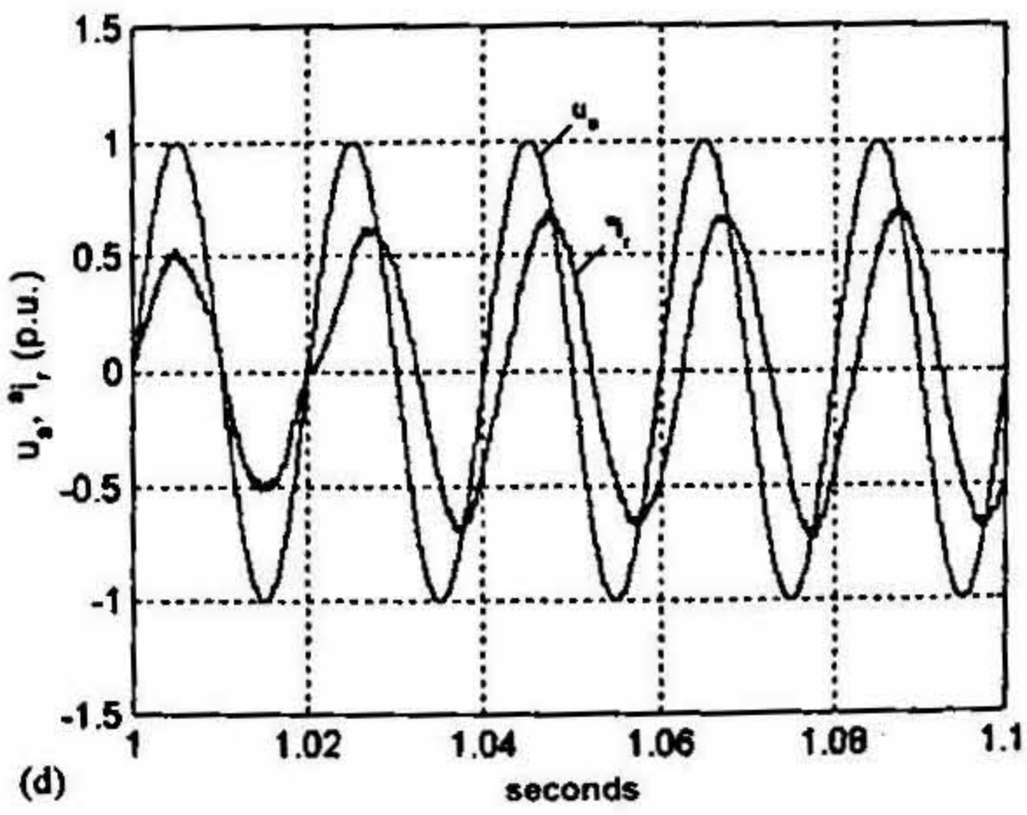

FIG. 13. Simulated step response of (a) i_{rd}, (b) i_{rq}, (c) i_r along with u_s and (d) $^s i_r$ along with u_s for the grid-connected SRIM.

In the implementation of the present scheme, it was felt that a single processor would be convenient to execute the control algorithms for the front end as well as the machine side converter. Several control loops, therefore, need to be executed in real time at a high sampling rate. This has prompted the use of computationally powerful digital signal processor (DSP) for the present application. The TMS320F240 DSP from Texas Instruments has the architectural features necessary for digital control functions and the peripherals needed to provide a single-chip solution for motor control applications. The present digital control hardware is built around the 'F240 processor. The TMS320F240 is a 16-bit, fixed-point DSP which can execute 20 million instructions per second (MIPS). It houses several advanced peripherals, optimized for motor control applications. The most important peripheral is the event manager (EV) module, which provides general-purpose timers and compare registers to generate up to 12 PWM outputs. Efficient usage of the EV timers reduces software overhead for PWM generation significantly. The EV incorporates a quadrature encoder pulse (QEP) circuit which can be interfaced directly to an incremental position encoder. The peripherals also include a dual, 10-bit analog-to-digital converter (ADC), which can perform two simultaneous conversions within 7 μs, an internal PLL clock module, a serial communication interface and a serial peripheral interface.

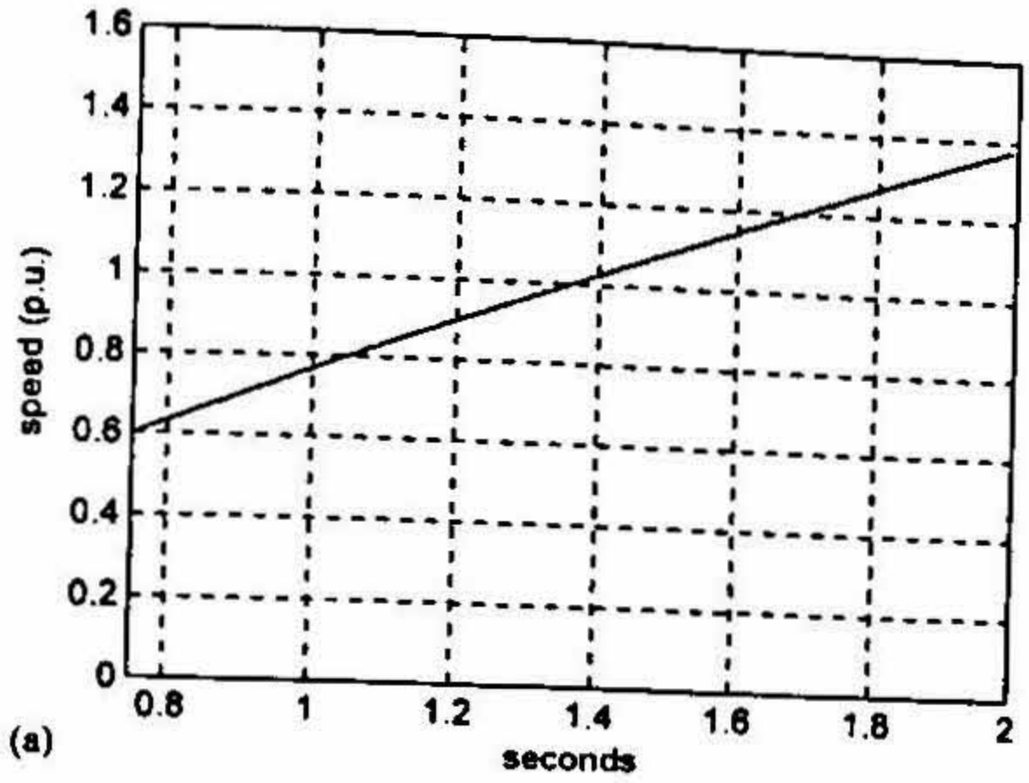

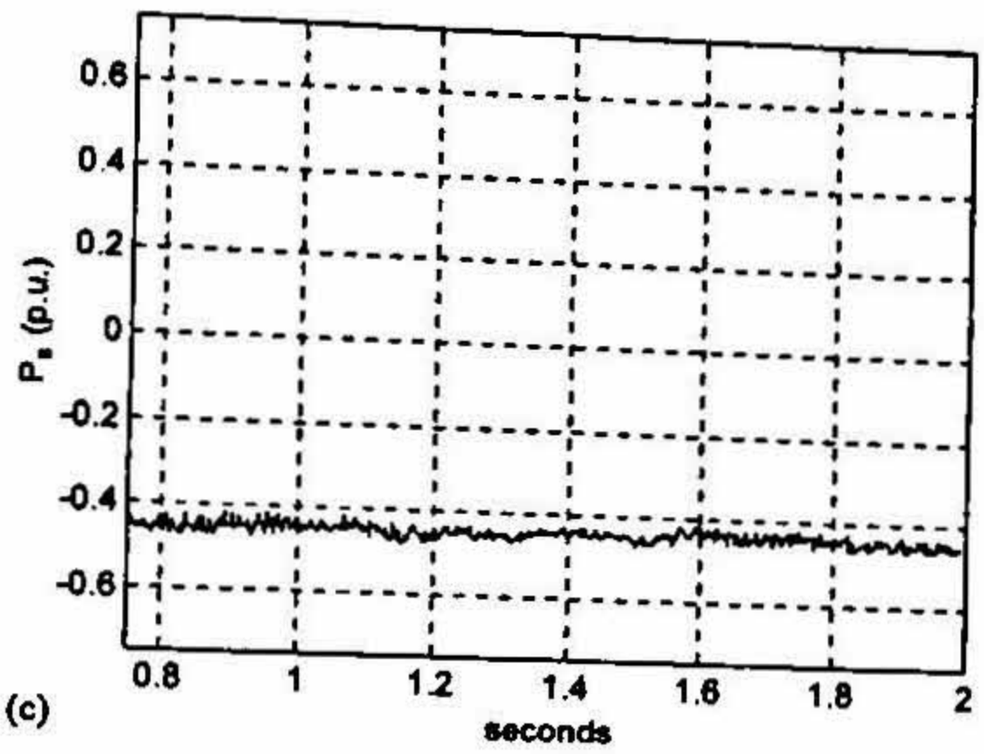

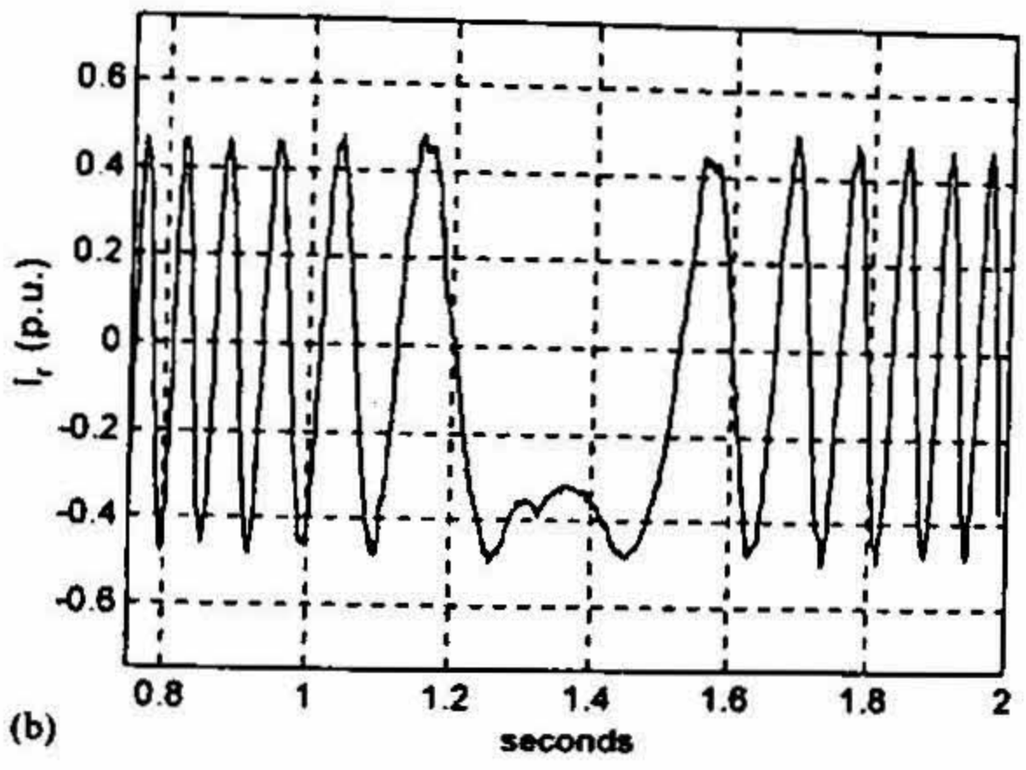

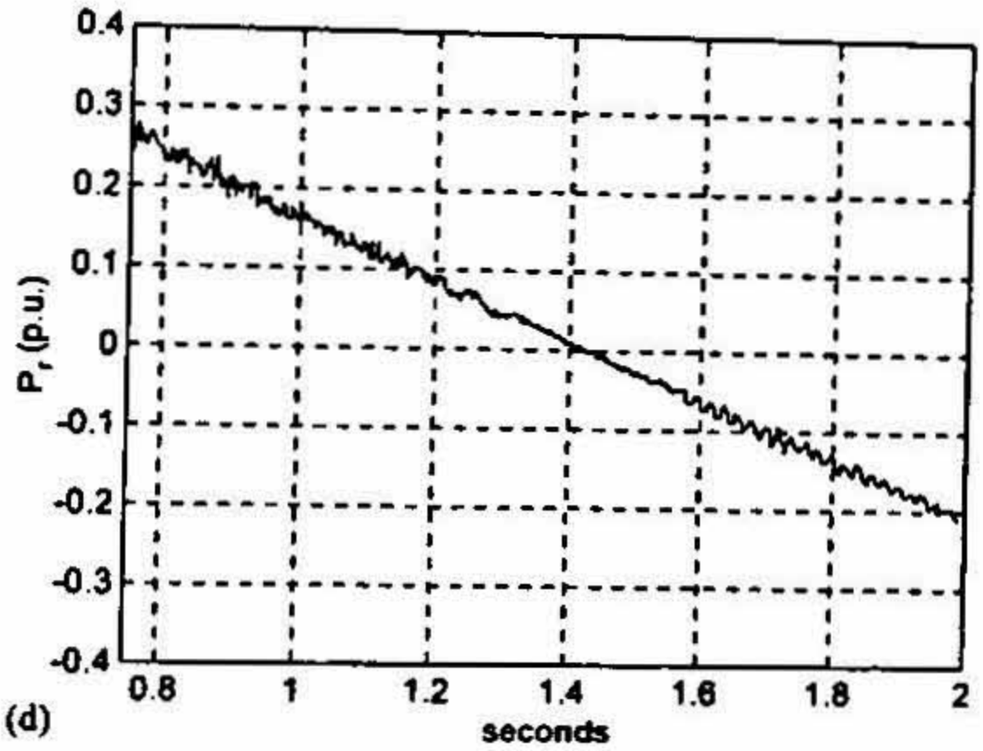

FIG. 14. Simulated response of (a) speed, (b) i_r, (c) stator power and (d) rotor power for the grid-connected SRIM.

A generalized digital control platform has been designed using TMS320F240. It comprises four hardware modules: (i) an analog signal conditioning board, (ii) a DSP board, (iii) a position encoder interface and (iv) a power converter interface. All these modules are developed in-house and the integrated platform is being used for different motor control applications. The schematic block diagram of the control hardware is given in Fig. 16.

The requirement for fast real-time control demands that the software has to be efficient in terms of execution time. This has prompted the use of Assembly Language for programming the DSP. All the functions that the processor needs to execute are first broadly grouped into different tasks. Each task comprises several subroutines. The tasks are arranged in an appropriate sequence in time, so that the required bandwidths of the different control loops can be achieved. This is done by a task scheduler. The task scheduler keeps track of the present task that is being executed and switches to the subsequent one at the next Timer1 interrupt. This is implemented by using a software counter.

The entire computation within the processor is done on a per unit scale. For a 16-bit processor, the (signed) maximum and minimum numbers vary from 7FFF h to 8000 h. This is taken as +2 p.u. to –2 p.u. Therefore, +1 p.u. is represented by 3FFF h, and –1 p.u. by 4000 h.

For outputting the different variables through the DAC (which is 12 bit), appropriate scaling of the variables is, therefore, necessary. In practice, the scaling is done in such a way that +10 V presents 2 p.u. scale. (Hence, most variables appear to be within +5 V).

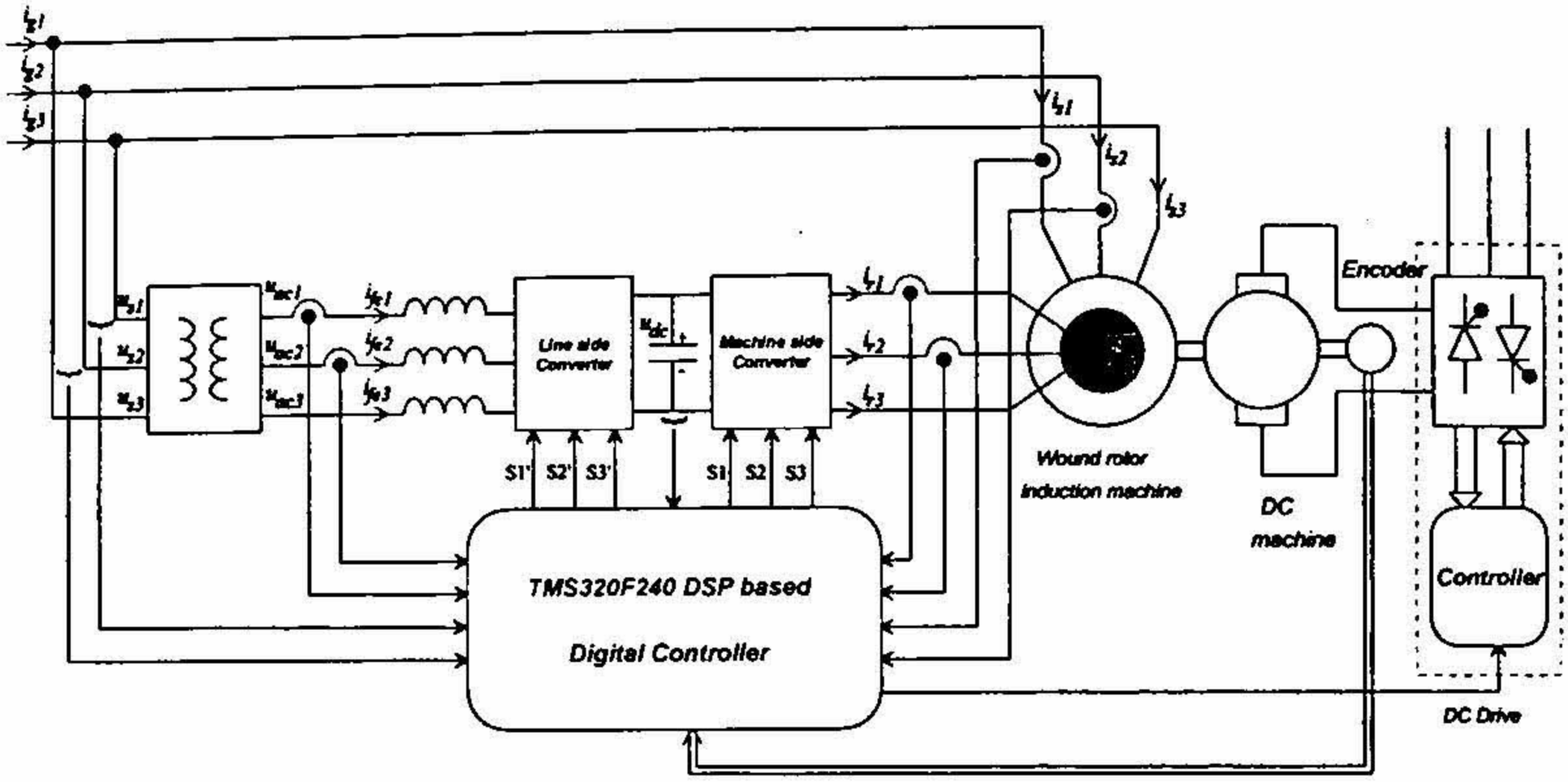

FIG. 15. Organization of the experimental set-up.

The step response of i_{rq} from 0 to 0.5 p.u. with i_{rd} held constant at 0.75 p.u. is shown in Fig. 17(a). The designed active current loop time constant is 1 ms. The corresponding stator current (i_s) and the rotor current in the stator reference frame ${}^{S}i_r$ are given in Figs 17(b) and (c), respectively. It is observed that when i_{rq} is zero, the stator current is close to zero and the rotor supplies the reactive power for the machine. With the application of positive i_{rq}, the stator instantly

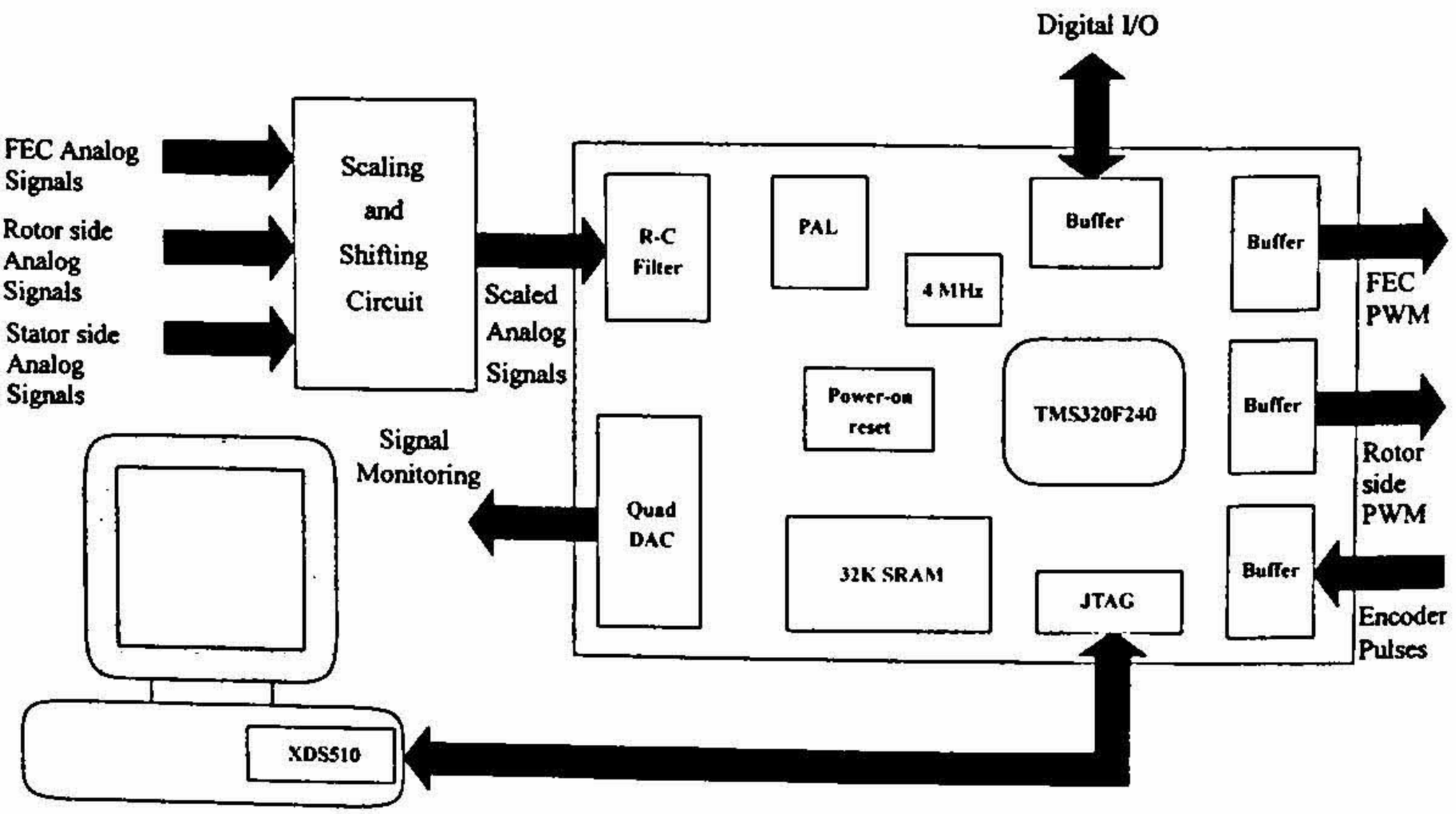

FIG. 16. Organization of the digital control hardware.

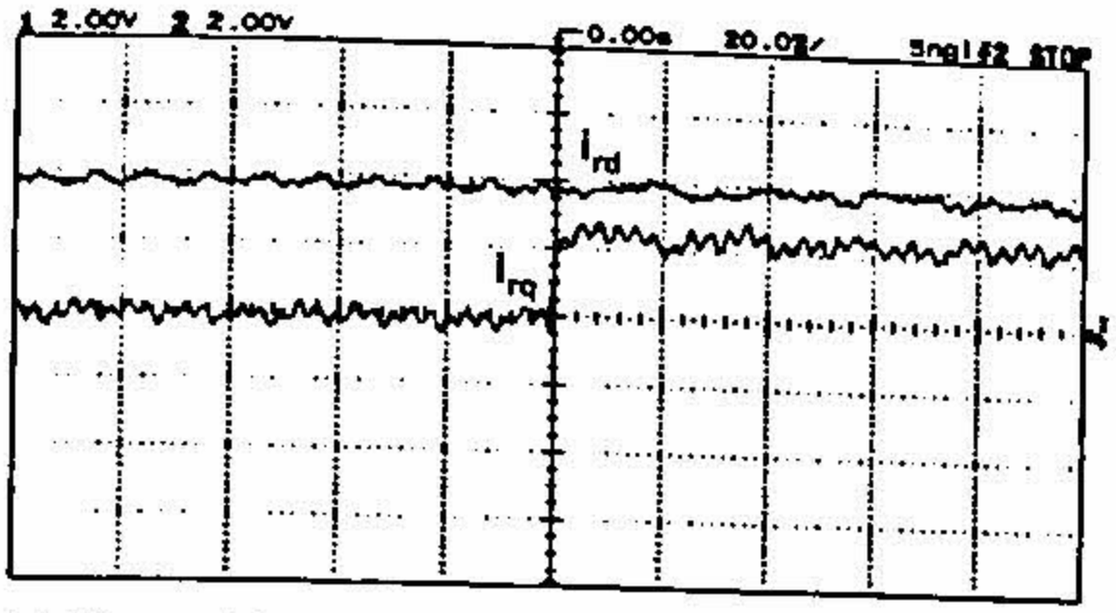

(a) Channel 1- i_{rd}, channel 2-irq

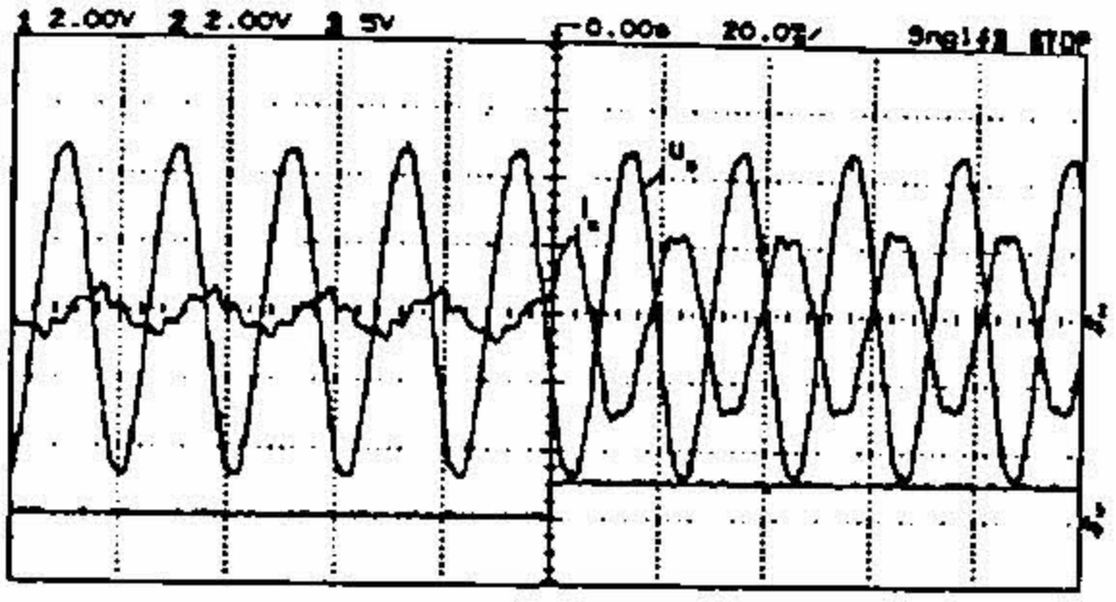

(b) Channel 1- u_S, channel 2-i_S, channel 3-i^*_{rq}

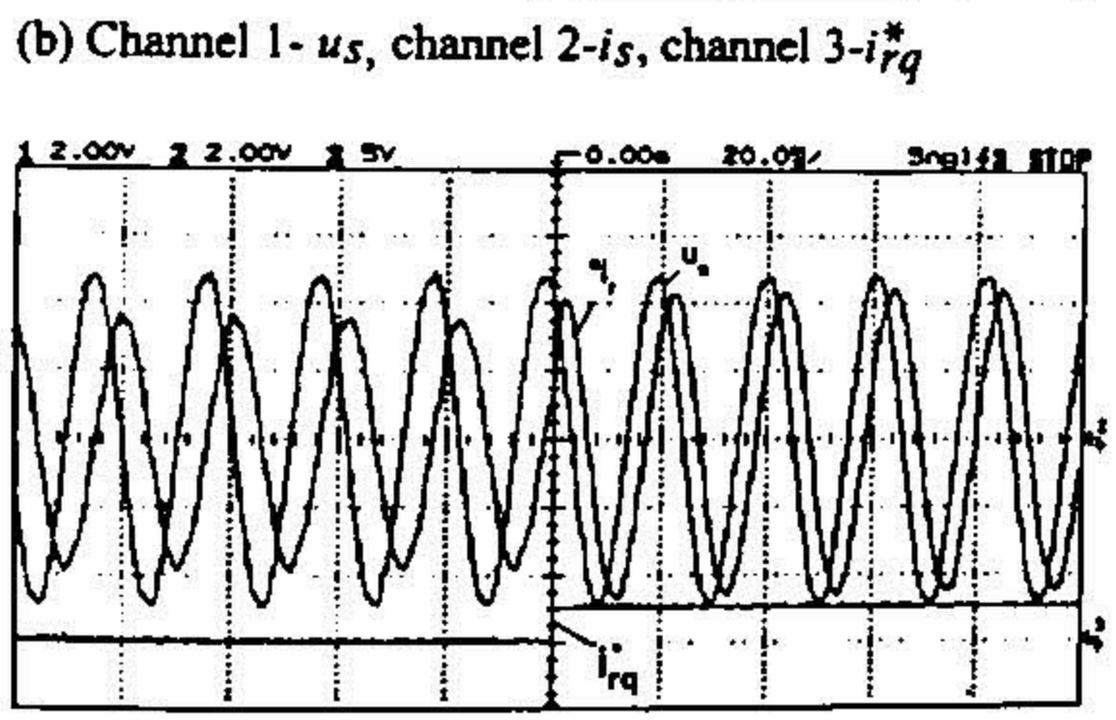

(c) Channel 1- u_S, channel 2-$^S i_r$, channel 3-i^*_{rq}

FIG. 17. Experimental results showing the transient response of the q-axis current control loop. A step in i^*_{rq} is given from 0 to 0.5 p.u. and i^*_{rd} is maintained at 0.75 p.u.

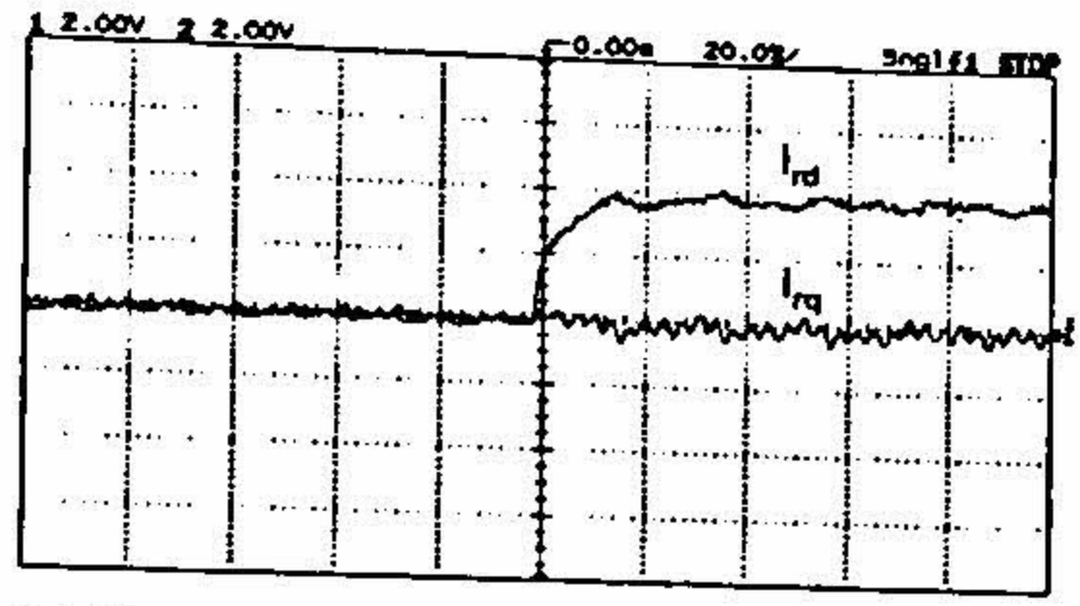

(a) Channel 1- i_{rd}, channel 2-irq

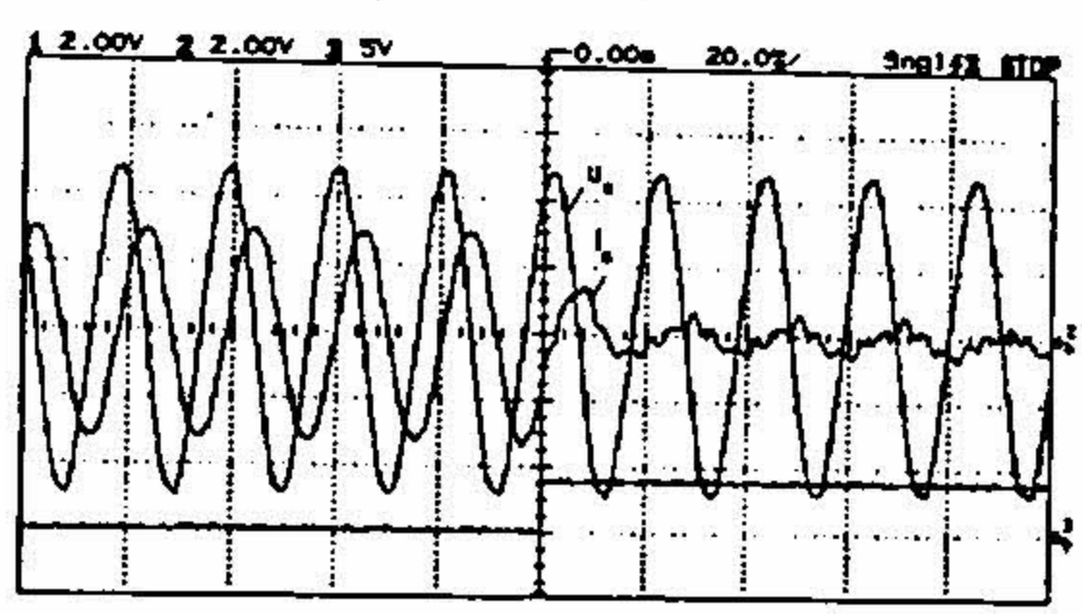

(b) Channel 1- u_S, channel 2-i_S, channel 3-i^*_{rd}

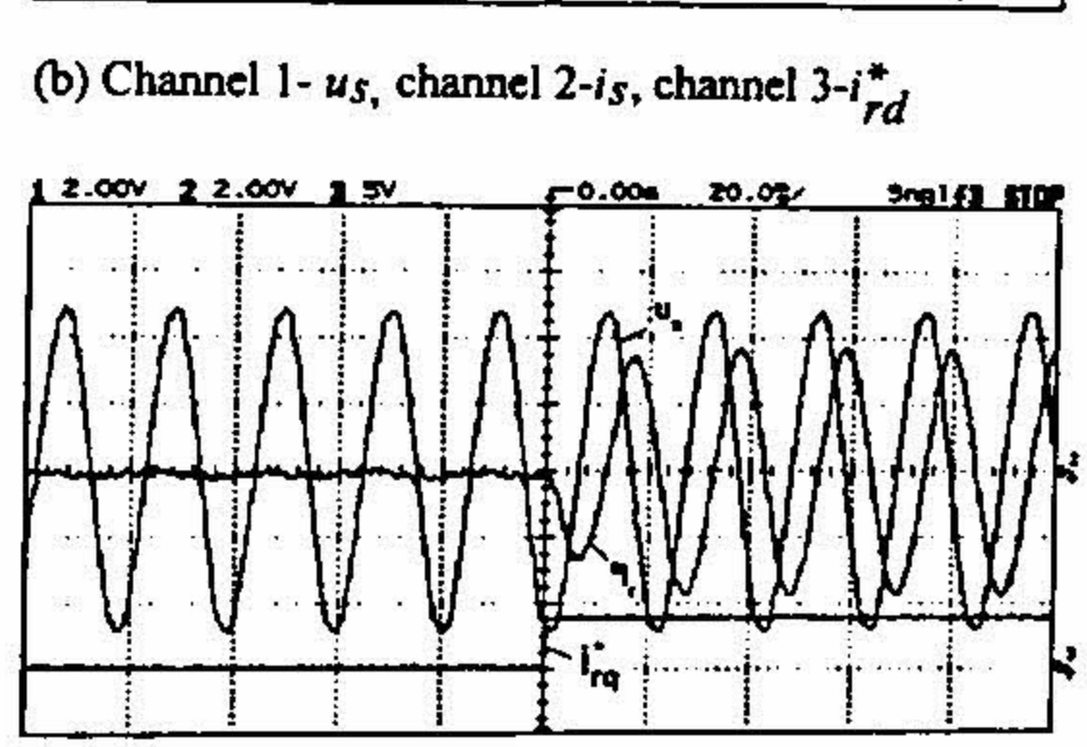

(c) Channel 1- u_S, channel 2-$^S i_r$, channel 3-i^*_{rd}

FIG. 18. Experimental results showing the transient response of the d-axis current control loop. A step in i^*_{rd} is given from 0 to 0.75 p.u. and i^*_{rq} is maintained at zero.

goes into generating mode (negative i_{sq}) at almost unity power factor. The rotor current increases in magnitude as it now handles both the active and reactive powers.

The dynamics of the reactive current loop is made slightly slower than the active loop. The reactive current reference is normally kept constant and is not decided by any outer loop. So the reactive loop is mostly regulatory in nature and need not be as fast as the active loop. In Fig. 18(a), the response of i_{rd}, when a step change in i^*_{rd} is given from 0 to 0.75 p.u., is presented. The active current reference i^*_{rq} is kept at zero. Figures 18(b) and (c) show that the stator initially supplies only the reactive power of the machine, and the rotor current is zero. With the application of i_{rd} the reactive power is transferred to the rotor circuit and the stator current falls close to zero.

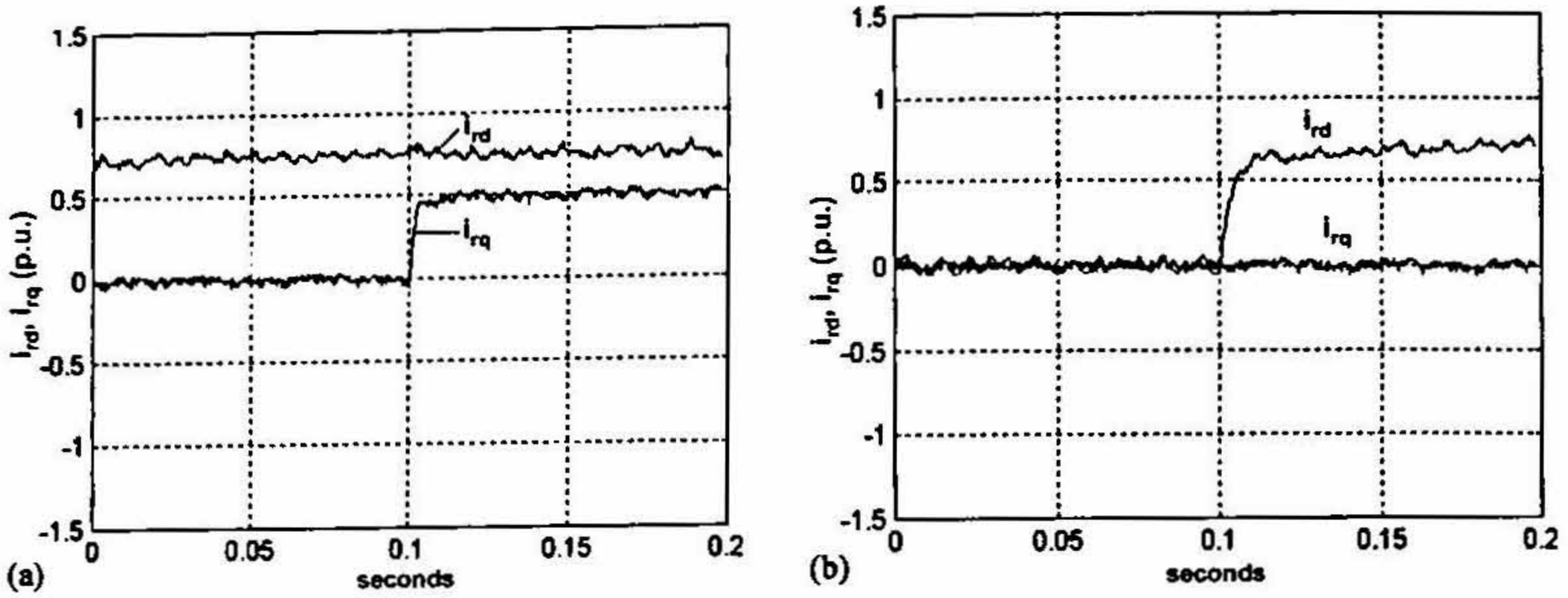

FIG. 19. Simulated response of i_{rd} and i_{rq} for step change of (a) i_{rq}^* from 0 to 0.5 p.u. with i_{rd}^* held constant at 0.75 p.u and (b) i_{rd}^* from 0 to 0.75 p.u. with i_{rq}^* held constant at zero.

The transient responses of these current loops obtained through simulation are also presented in Figs 19(a) and (b). It is observed that zthe simulation and experimental results are in good agreement thereby validating the machine modelling and design of the controller.

The relationship between the stator and rotor currents in the d- and q-axes is shown clearly in Figs 20(a) and (b). Along the q-axis, i_{rq} and i_{sq} are proportional to each other differing by a factor $(1 + \sigma_s)$, but of opposite polarity. However, along the d-axis, when i_{rd} is zero, i_{sd} equals $i_{ms}/(1 + \sigma_s)$. With the application of i_{rd}, the reactive power is transferred to the rotor circuit and i_{sd} falls down to zero. The steady-state relation between $u_{s\alpha}$ and $i_{ms\alpha}$ is shown in Fig. 20(c). It is obvious that $i_{ms\alpha}$ lags the supply voltage component by 90°. The steady-state value of i_{ms} is also shown in the same plot.

The stator and rotor currents in their own reference frames, for subsynchronous and synchronous operations, are shown in Figs 21(a) and (b). The rotor current under synchronous condition is DC and the operation is observed to be perfectly stable. The ride through synchronous speed is illustrated in Fig. 21(c). The rotor current waveform passes through zero frequency from one phase sequence to the other.

8. Conclusion

A stator flux-oriented model has been derived for the wound rotor induction machine. Current controllers designed in the field reference frame comprise proportional or proportional integral controllers with subsequent addition or subtraction of the compensating terms. The design method is simple as it directly follows from the rotor voltage equations. Simulation results show that the dynamics of the active and reactive current loops are decoupled as required.

A power hardware platform for implementing the rotor side control strategies has been built. The hardware is designed in a modular fashion and has been standardized in the laboratory for general motor control applications. A TMS320F240 DSP-based digital control board is also designed and developed. This platform is powerful enough to execute all the control loops associated with rotor side control and front-end converter control. Field-oriented control using

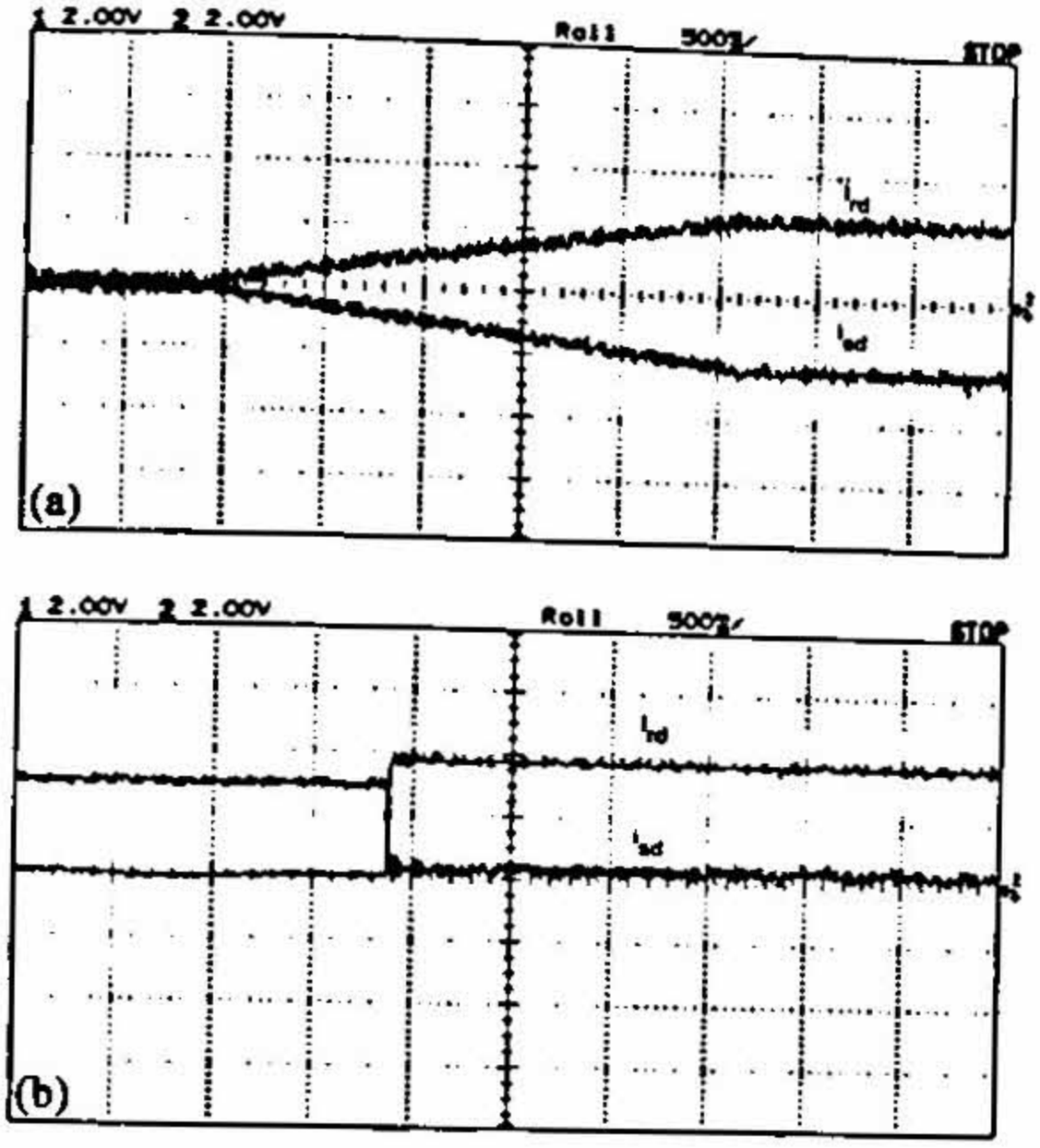

FIG. 20. Experimental results showing relationship between (a) i_{rq} and i_{sq} (b) i_{rd} and i_{sd}, and (c) u_{sa} and i_{msa}.

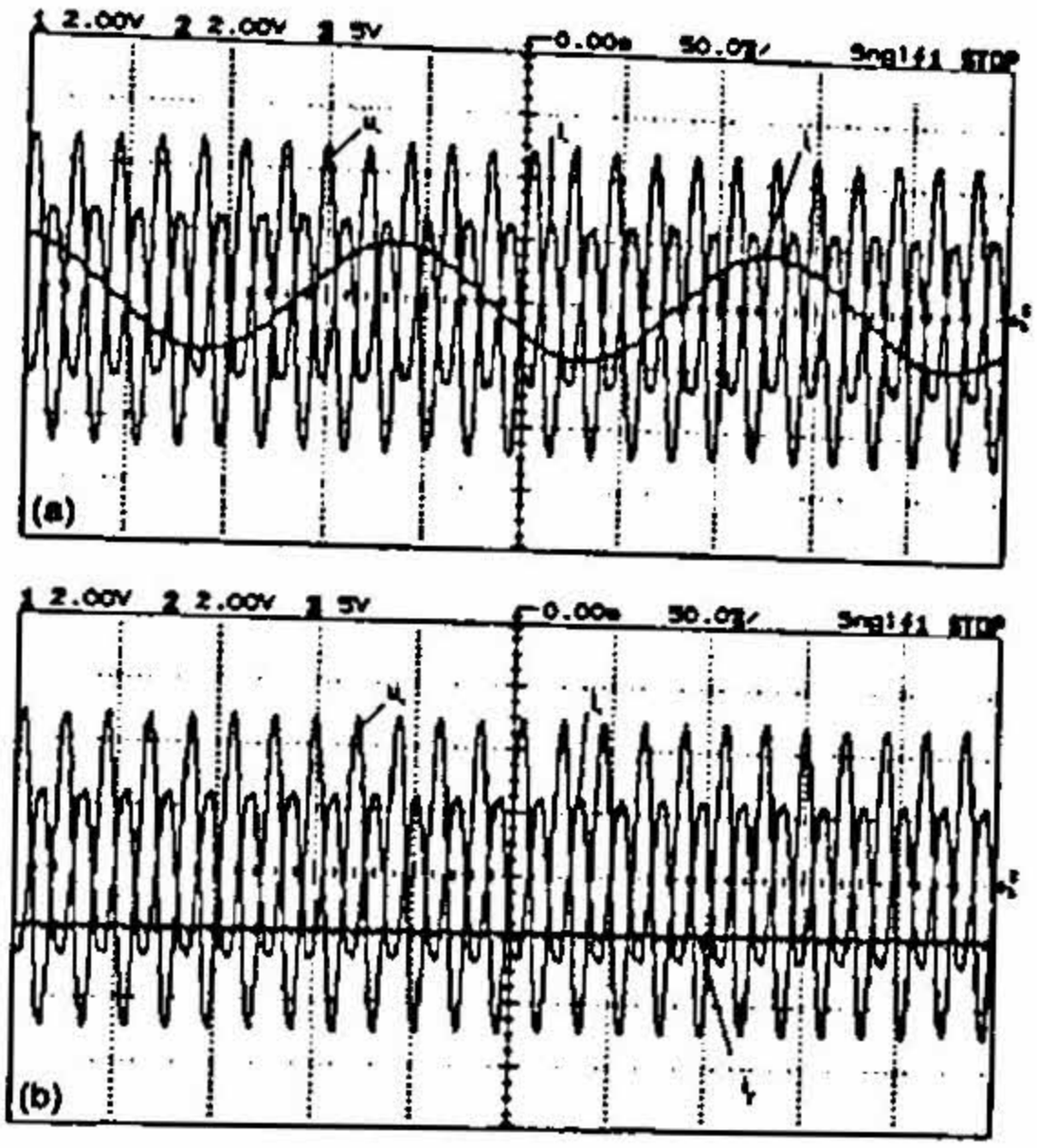

FIG. 21. Experimental results showing steady-state waveforms for $i_{rq}^{*} = 0.75$, $i_{rd}^{*} = 0.5$ (a) at 1275 rpm (sub-synchronous), (b) at 1435 rpm (synchronous) and (c) transition through synchronous speed.

shaft position sensor is implemented. Experimental results presented show decoupled response for the active and reactive current loops. They are also in close agreement with the simulated waveforms.

References

1. SEN, P. C. AND MA, K. H. J. — Rotor chopper control for induction motor drive: TRC strategy, *IEEE Trans.*, 1975, IA-11, 43-49.
2. ERLICKI, M. S. — Inverter rotor drive of an induction machine, *IEEE Trans.*, 1965, PAS-84, 1011–1016.
3. LAVI, A. AND POLGE, R. J. — Induction motor speed control with static inverter in the rotor, *IEEE Trans.*, 1966, PAS-85, 76–84.
4. SHEPHERD, W. AND STANWAY, J. — Slip power recovery in an induction motor by the use of a thyristor inverter, *IEEE Trans.*, 1969, IGA-5, 74–82.
5. WAKABAYASHI, T., HORI, T., SHIMZU, K. AND YOSHIOKA, T. — Commutatorless Kramer control system for large capacity induction motors for driving water service pumps, *IEEE/IAS Annual Meet*, 1976, pp. 822–828.

6. LONG, W. E. AND SCHMITZ, N. L. Cycloconverter control of the doubly fed induction motor, *IEEE Trans.*, 1971, IGA-7, 95–100.

7. WEISS, H. W. Adjustable speed AC drive systems for pump and compressor applications, *IEEE Trans.*, 1974, IA-10, 162–167.

8. CHATTOPADHYAY, A. An adjustable-speed induction motor drive with a cycloconverter-type thyristor-commutator in the rotor, *IEEE Trans.*, 1978, IA-14, 116–122.

9. MAYER, C. B. High response control of stator watts and vars for large wound rotor induction motor adjustable speed drives, *IEEE/IAS Annual Meet*, 1979, pp. 817–823.

10. LEONHARD, W. *Control of electrical drives*, Springer-Verlag, 1985.

11. VAS, P. *Sensorless vector and direct torque control*, Oxford University Press, 1998.